J. Math. Biol. (1992) 31: 25–71

Journal of Mathematical Biology

Analysis of dynamic and stationary pattern formation in the cell cortex

M. A. Lewis[1,2*] and J. D. Murray[1]

[1] Department of Applied Mathematics, FS-20, University of Washington, Seattle, Washington, 98195, USA

[2] Department of Zoology, NJ-15, University of Washington, Seattle, Washington, 98195, USA

Received May 6, 1991; in revised form August 15, 1991

Abstract. We study a sol-gel mechanochemical model for cellular cytoplasm. Using conservation equations and a force balance equation, we derive equations for the sol-gel dynamics. Regular perturbation analysis suggests the growth of patterns which may be either dynamic or stationary, depending on parameter values. Nonlinear analysis, which indicates that these patterns remain bounded, is confirmed by numerically solving the mechanochemical equations. We use these analytical and numerical results to model two different biological problems: the dynamic formation of filopodia in nerve growth cones, and the growth of microvilli in epithelial cells.

Key words: Cytoplasm – Mechanochemical Sol-gel – Microvilli – Filopodia

1 Introduction

Highly organized patterns are often evident on the surface of cells that have contractile actin-dense cortices. These may be stationary structures such as microvilli and stereocilia (see, for example, Alberts 1983) or may extrude dynamically from the cell surface as ruffles, blebs, microspikes and filopodia (see, for example, Bray and White 1988); see also Figs. 18 and 19 below. These structures have diverse functions that include increasing the absorbent area of the intestine (microvilli), transmitting acoustic impulses in the ear (stereocilia) and guiding the young nerve growth cone up haptotactic gradients (via filopodia).

The actin protein undergoes a dynamic sol-gel phase change that is thought to be the crucial feature governing its contractile activity (Taylor et al. 1979; Condeelis 1983; Oster and Odell 1984a,b). Interacting with the actin filaments are five different classes of protein with various levels of calcium sensitivity (Alberts et al. 1983) (Fig. 1). Gel forming (or actin binding) proteins cross-link the actin filaments into a mesh or actin gel (Stossel 1983). This polymer gel is closely interwoven with the stable elements and is thereby linked to the cell structure. Bundling proteins stabilize the gelled actin filaments into isotropic networks

* *Present address:* Department of Mathematics, University of Utah, Salt Lake City, UT 84112, USA

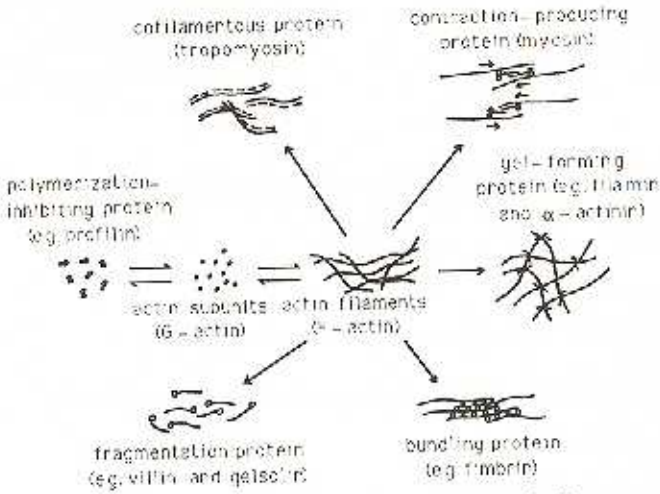

Fig. 1. Proteins affecting the actin cytoskeleton. Schematic diagram summarizing the effect of various actin-binding proteins on the actin cytoskeleton. (Based on Alberts et al. 1983)

(Weeds 1982). Fragmenting proteins, which cleave the actin filaments at mid-point between the cross-links, break the gel up into sol (Stossel 1983). The actin filaments are then in a dynamic equilibrium. This equilibrium is critically affected by the levels of free calcium. At lower calcium levels, the actin remains as a gel, but as levels of calcium rise from $10^{-7}M$ to $10^{-6}M$, the sol phase predominates.

Oster et al. (1985) and Oster and Odell (1984b) suggested that it is this sol-gel phase transition which is a key factor in coordinating the formation of stationary structural patterns on the cell cortex. We suggest that, in addition, the sol-gel phase transition gives rise to important dynamic structural patterns. This is borne out by the analysis presented here.

Our investigation involves a mathematical model for actomyosin gels. Rather than starting with a detailed microscopic model, we use the continuum mechanics approach to model the macroscopic viscoelastic properties of the cytogel (see, for example, Oster and Odell 1984a,b; Oster 1984; Odell 1984; Oster et al. 1985): experimentally measurable mechanical properties of the cytogel are used in establishing its constitutive behaviour. By characterising properties of such a viscosity, elasticity, osmotic stress and contractile stress, we can describe the dynamic behaviour of the cytogel through the use of force balance and mass conservation equations.

Our model uses two reaction-diffusion-convection type equations to describe the chemical kinetics and one tensor equation to describe the balance of forces within the cytogel (Sect. 2). Linear analysis of these equations shows how spatial patterns can arise when disturbances of a critical wave length grow away from the homogeneous steady state solution (Sect. 3). The growth of these modes is bounded by nonlinear terms and a new heterogeneous steady state evolves (Sect. 4). While relating closely to a simpler two-equation model which was proposed by Oster et al. (1985), our system exhibits long-term dispersive wave patterns which are not evident from the simpler model. In Sect. 5 we show that such enhanced pattern-forming capabilities, such as the extrusion of filopodia from nerve growth cones, are also found in nature, indicating that the model represents a useful extension to that of Oster et al. (1985).

Clearly, the complexity of the microscopic and chemical structure of the cytogel means that such a system of equations cannot describe precisely the current state in a given cell. Rather, its purpose is to provide a theoretical framework with which the basic mechanisms that prevail during cortical differentiation and movement can be understood.

2 The mechanics of actin gels

Cytoskeletal fibres fall into three main categories: actin filaments, microtubules and intermediate filaments. In the presence of a phosphorylated myosin, actin filaments can form contractile units and provide a basis for cellular movement and reorganization. By way of contrast, microtubles and intermediate filaments provide no contraction, but are the structural units for maintaining rigidity and cell shape. While microtubules assemble and disassemble according to cellular dynamics, intermediate filaments are highly stable and are the least soluble components (Alberts et al. 1983). The microtubules and intermediate filaments are loosely referred to as *stable elements*, while the actin mesh is the *contractile element*. Collectively, they give the cytoskeleton its mechanical properties.

2.1 A balance of forces determines the mechanical equilibrium

We now consider the sum total of the forces acting on an isolated piece of stationary cytogel which is in mechanical equilibrium. It is able to maintain its shape because of a balance of several forces:

1. the active contractile forces generated by the actomyosin complex

2. the passive elastic restoring forces arising from the stable elements and from the actin gel

3. the osmotic pressure of the cytogel.

The cytogel is a distributed osmometer (as opposed to a membrane osmometer) because each volume element establishes an osmotic equilibrium with its surroundings. The osmotic pressure, resulting from electrostatic repulsions, polymer/solvent interactions and mixing interactions (Oster 1984), provides an expansive force.

The passive elastic forces provided by the stable elements are long-range restorative forces which counteract strains and re-establish the previous shape of the cell. By contrast, the elastic forces generated by the actin gel result from the thermal motions of the fibres (Tanaka 1981) and provide short-range restoring forces which counteract stretching (dilation) and compression.

2.2 Sol-gel dynamics

We start with a phenomenological relationship which forms the basis for the 'solation-contraction' hypothesis (Taylor 1979). We expect an unstrained cytogel unit to be in equilibrium sol-gel balance – in the absence of elastic forces, the osmotic and contractile forces balance. If cytosolic calcium levels decrease, the

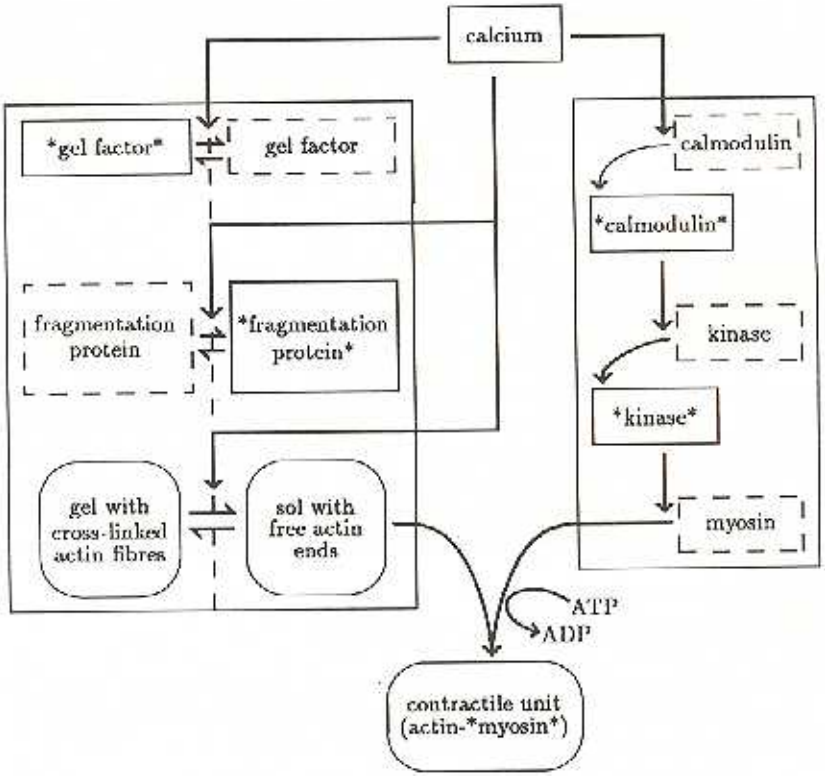

Fig. 2. Calcium mediated solation and contraction of cytogel. This diagrammatic representation shows the essential features of the solation-contraction hypothesis. Calcium mediates both solation and the assembly of contractile units. Activation of the myosin protein in the contractile unit is through the dephosphorylation of ATP (adenosine triphosphate) to ADP (adenosine diphosphate). (Asterisks indicate activated complexes.) Supercritical calcium concentrations cause partial solation and the construction of contractile units

gel concentration increases while osmotic forces overcome the opposing contractile and elastic forces and the cytogel dilates. If cytosolic calcium levels rise, the cytogel unit solates while contractile forces surpass the opposing elastic and osmotic forces and the cytogel contracts (Fig. 2). Dilation and calcium levels correlate negatively and only the dilation is used in our phenomenological model. This relationship between the dilation and the sol-gel dynamics is shown in Fig. 3.

We define S to be the concentration of sol and G to be the concentration of gel. Thus, for a spatially homogeneous strip of cytogel, the sol-gel dynamics can be written as

$$\frac{\partial S}{\partial t} = -k_+(\theta)S + k_-(\theta)G \tag{1}$$

$$\frac{\partial G}{\partial t} = k_-(\theta)S - k_-(\theta)G, \tag{2}$$

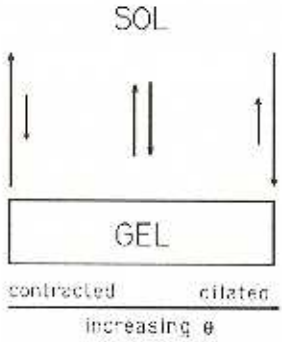

Fig. 3. Dilation regulates sol-gel dynamics. Unstrained gel is in chemical equilibrium with the sol. When the cytoplasm contracts, the dynamic balance shifts so as to increase sol concentration while cytoplasmic dilation shifts the balance towards increased gel concentration

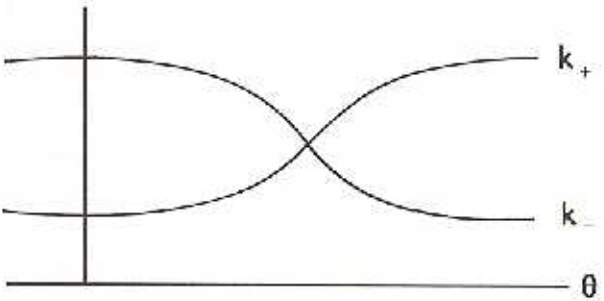

Fig. 4. The sol-gel dynamics as a function of dilation. The gelation rate (k_+) and solation rate (k_-) are given as qualitative functions of the dilation, θ

where $k_+(\theta)$ and $k_-(\theta)$ have the qualitative form shown in Fig. 4 and θ is the dilation, or measure of stretching, given by

$$\theta = \nabla \cdot \boldsymbol{u}, \tag{3}$$

$\boldsymbol{u}$ being the distance that the stable elements of cytoskeleton have been displaced from their original unstrained position.

2.3 Stress-strain relationships in the cytogel

We extend our discussion to include cytogel dynamics giving rise to spatial heterogeneities in higher space dimensions. In Sec. 2.2 we saw that an isolated piece of stationary cytogel was able to maintain its shape through the balance of expansive and contractile forces. The key to understanding cytogel dynamics is provided by an analogous equation which accounts for the time-dependent cytogel movements in three spatial dimensions.

We expect cytogel mechanisms to adhere (at this level of modelling) to Newtonian dynamics. For cellular processes, the inertial terms are negligible compared with viscous and elastic forces (Oster et al. 1983); motion ceases as soon as the applied forces are turned off (Purcell 1977). Therefore, at any given time, the mechanical forces acting upon the cytogel must balance, reflecting the following equilibrium condition:

$$\boldsymbol{F} = \nabla \cdot \boldsymbol{\sigma} = \boldsymbol{0}, \tag{4}$$

where $\boldsymbol{F}$ is the force vector and $\boldsymbol{\sigma}$ is the stress tensor. Thus, in conjunction with Eq. (4), the stress-strain relationships for the elastic, viscous, contractile and

osmotic forces will lead to a force balance equation describing the cytogel dynamics. We consider each of the elastic, viscous, contractile and osmotic stress-strain relationships in turn.

Although microscopic evidence, such as immunofluorescence micrographs, indicates anisotropy in cytoskeletal structure, we choose the simplest possible case and model the actin gel as having isotropic elastic properties. By measuring the force taken to stretch the gel in a given direction, one can generate a mechanical response curve relating the elastic uni-directional stress to the dilation. This relationship is linear for small strains, but becomes nonlinear as gel fibres align and eventually tear when the dilation increases (Oster and Odell 1984a). Because we will primarily be concerned with the small strain cytoplasmic behaviour, we use linear theory for our sol-gel model. This is expressed empirically by Hooke's Law, which relates *short-range* elastic stresses, such as those arising from the actin gel, to the strain (Lur'e 1964). Strains will also incur a long-range elastic response, however, when the fibrous stable elements transmit non-local strains. Because elasticity is a property of the actin gel, we expect the elastic response of the cytoplasm to be proportional to the gel concentration. Thus, adding a long-range elastic response (see, for example, Oster et al. 1985; Murray 1989; Lewis 1990) to Hooke's Law and multiplying by the normalized gel concentration, the elastic stress tensor is taken to be

$$\boldsymbol{\sigma}_E = \gamma \frac{G}{c_0} (\boldsymbol{\epsilon} - \beta \Lambda \boldsymbol{\epsilon} + \hat{\nu}(\theta - \beta \Lambda \theta)\boldsymbol{I}), \tag{5}$$

where $\boldsymbol{\epsilon} = (\nabla \boldsymbol{u} + \boldsymbol{u}\nabla)/2$ is the strain tensor, $\gamma = E/(1+\nu)$, $\hat{\nu} = \nu/(1-2\nu)$, with E the effective elastic modulus and ν the Poisson ratio, $\beta \geqslant 0$ is a measure of the long-range elasticity and c_0 is the cytogel density, measured at $\theta = 0$.

The viscosity of the sol phase is far less than that of the gel phase, leading us to expect that the viscous response of the cytoplasm is proportional to the gel concentration. Multiplying the viscous stress tensor (Landau and Lifshitz 1970) by the normalized gel concentration yields

$$\boldsymbol{\sigma}_V = \frac{G}{c_0} (\mu_1 \boldsymbol{\epsilon}_t + \mu_2 \theta_t \boldsymbol{I}), \tag{6}$$

where μ_1 and μ_2 are the shear and bulk viscosities of the gel, respectively.

We expect a contractile stress, $\boldsymbol{\sigma}_A$, resulting from the complexing of myosin oligomers with the partially solated actin gel. Contraction of the gel leads to increased fibre concentrations and more myosin cross-bridges, thereby resulting in an increased contractile strength (Oster et al. 1983). This is an important mechanical characteristic of cytogel: as it contracts, it gets stronger. However, the cytogel cannot contract indefinitely; the sliding filament mechanism can no longer contract when the filaments are fully overlapping. Highly contracted cytogel ultimately loses its ability to contract (Fig. 5).

The traction per fibre will be a function of the availability of activated myosin oligomers. This in turn, depends on a myriad of secondary factors (see, for example, Lewis 1990). To keep our model as simple as possible we assume that there is an ample supply of activated myosin oligomers. As contraction occurs in the partially solated gel, we assume that the contractile stress is approximately proportional to the gel concentration. Thus we model the contractile stress tensor as

$$\boldsymbol{\sigma}_A = \frac{G}{c_0} \tau(\theta)\boldsymbol{I}. \tag{7}$$

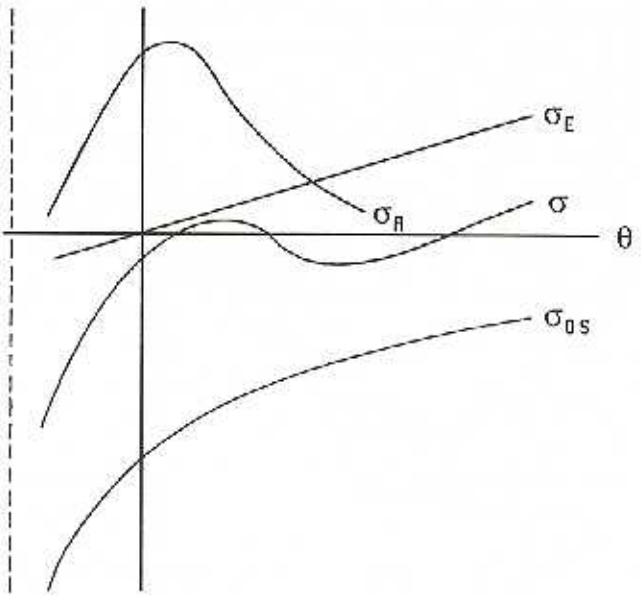

Fig. 5. Stress-strain relationship for actin gel. This shows the qualitative form of the stress-strain relationship for the actin gel. Ignoring sol-gel dynamics (1) (2), the relationship is shown for a constant gel concentration. Here σ_E is the elastic stress, σ_A is the contractile or active stress, σ_{OS} is the osmotic stress and σ is the total stress response

The function $\tau(\theta)$ models the dilation-dependent contractile strength described above (Fig. 5).

The osmotic stress components, including electrostatic repulsions, polymer/solvent interactions and mixing interactions (Oster 1984), become less potent as the cytogel dilates, giving a monotonically decreasing relationship between the osmotic stress and the dilation. Thus we model the osmotic stress tensor as

$$\boldsymbol{\sigma}_{OS} = -\pi(\theta)\boldsymbol{I}, \tag{8}$$

where $\pi(\theta)$ is shown in Fig. 5.

2.4 Model formulation

Including diffusive and convective sol-gel fluxes into the sol and gel equations (1)–(2) and the stress components (5), (6), (7) and (8) into the force balance equation (4) gives

$$\frac{\partial S}{\partial t} + \nabla \cdot \left(S \frac{\partial \boldsymbol{u}}{\partial t} \right) - D_S \Delta S + k_-(\theta) S - k_-(\theta) G = 0 \tag{9}$$

$$\frac{\partial G}{\partial t} + \nabla \cdot \left(G \frac{\partial \boldsymbol{u}}{\partial t} \right) - D_G \Delta G - k_+(\theta) S + k_-(\theta) G = 0 \tag{10}$$

$$\nabla \cdot (\boldsymbol{\sigma}_V + \boldsymbol{\sigma}_E + \boldsymbol{\sigma}_A + \boldsymbol{\sigma}_{OS}) = \boldsymbol{0}, \tag{11}$$

where D_S and D_G are the diffusion coefficients for the sol and gel respectively.

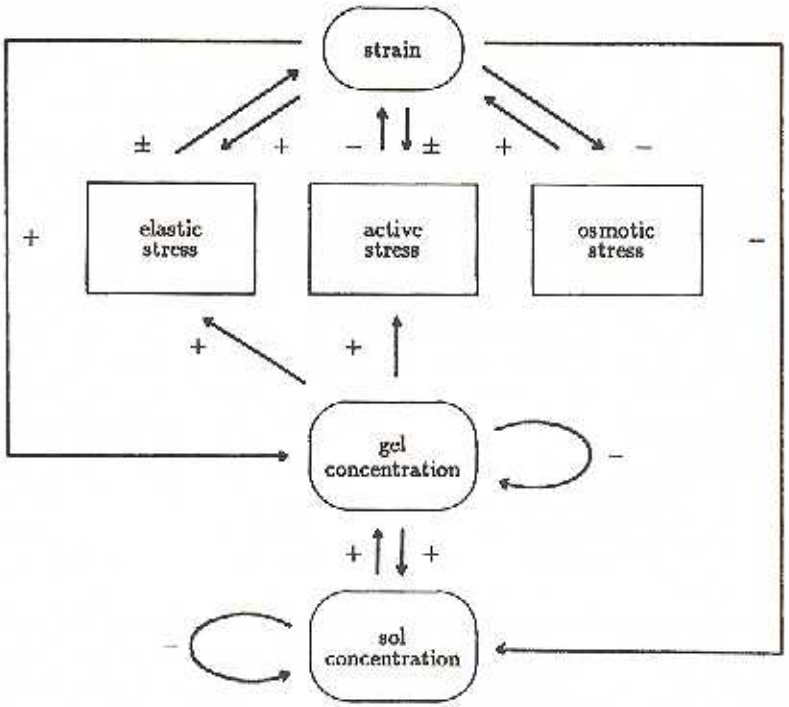

Fig. 6. Feed-back regulation of the sol-gel model

The feed-back mechanisms regulating the behaviour of (9)–(11) are shown diagramatically in Fig. 6.

The boundary conditions for (9)–(11) are derived from physical constraints on the system. These are also formulated as conservation laws.

First, the fibrous network of passive elements should not pass through the domain boundary, $\partial\Omega$. So

$$\boldsymbol{n} \cdot \frac{\partial \boldsymbol{u}}{\partial t} = 0 \quad \text{on } \partial\Omega, \tag{12}$$

where $\boldsymbol{n}$ is the outward drawn oriented unit normal to $\partial\Omega$. Integration over the surface of $\partial\Omega$, integration with respect to time and application of the divergence theorem yields a conservation law for θ:

$$\int_{\Omega} \theta \, dV = \Psi_0 \quad (\text{constant}), \tag{13}$$

where Ω is the solution domain.

Second, the total amount of sol plus gel present in the system should remain constant, reflecting conservation for the sol-gel system. Thus

$$\int_{\Omega} (S + G) \, dV = \Phi_0 \quad (\text{constant}). \tag{14}$$

This is facilitated by Neumann boundary conditions for S and G:

$$\boldsymbol{n} \cdot \nabla S = 0 \quad \text{on } \partial\Omega \tag{15}$$

and

$$\boldsymbol{n} \cdot \nabla G = 0 \quad \text{on } \partial\Omega. \tag{16}$$

Adding Eqs. (9) and (10), applying the divergence theorem, using the boundary conditions (12), (15) and (16), and integrating with respect to time, we obtain the conservation law (14).

The spatially homogeneous one-dimensional analogue of (9)–(10) is

$$\frac{\partial S}{\partial t} + S\frac{\partial \theta}{\partial t} + k_-(\theta)S - k_-(\theta)G = 0 \tag{17}$$

$$\frac{\partial G}{\partial t} + G\frac{\partial \theta}{\partial t} - k_-(\theta)S + k_-(\theta)G = 0 \tag{18}$$

which imply

$$S + G = (S + G)|_{\theta=0}\exp(-\theta) = c_0\exp(-\theta). \tag{19}$$

The conservation law (13) constrains the dilation to remain constant at $\theta = \theta_0$, while (14) and (19) require that $S + G = S_0 + G_0 = c_0\exp(-\theta_0)$. Thus (17)–(18) has a stable steady state,

$$S_0 = \frac{k_-(\theta_0)c_0\exp(-\theta_0)}{k_+(\theta_0) + k_-(\theta_0)}$$

$$G_0 = \frac{k_+(\theta_0)c_0\exp(-\theta_0)}{k_+(\theta_0) + k_-(\theta_0)}.$$

We nondimensionalise the system (9)–(11) so that G is unity at the uniform steady state. Our new variables are

$$S^* = \frac{S}{G_0}, \qquad G^* = \frac{G}{G_0}, \qquad u^* = u\sqrt{\frac{\tilde{\nu}}{\mu D_S}},$$

$$t^* = \frac{t\tilde{\nu}}{\mu}, \qquad x^* = x\sqrt{\frac{\tilde{\nu}}{\mu D_S}}, \qquad D^* = \frac{D_G}{D_S}, \qquad \beta^* = \frac{\tilde{\nu}\beta}{\mu D_S} \tag{20}$$

$$k_+^* = \frac{k_+\mu}{\tilde{\nu}}, \qquad k_-^* = \frac{k_-\mu}{\tilde{\nu}}, \qquad \tau^* = \frac{\tau}{\tilde{\nu}}, \qquad \pi^* = \frac{\pi c_0}{G_0\tilde{\nu}},$$

where $\mu = \mu_1 + \mu_2$ and $\tilde{\nu} = \gamma(1 + \hat{\nu})$.

Substituting these quantities into (9)–(11), and dropping the asterisks for notational simplicity, we obtain in one dimension

$$\frac{\partial S}{\partial t} + \frac{\partial}{\partial x}\left(S\frac{\partial u}{\partial t}\right) - \frac{\partial^2 S}{\partial x^2} + F(S, G, \theta) = 0 \tag{21}$$

$$\frac{\partial G}{\partial t} + \frac{\partial}{\partial x}\left(G\frac{\partial u}{\partial t}\right) - D\frac{\partial^2 G}{\partial x^2} - F(S, G, \theta) = 0 \tag{22}$$

$$\frac{\partial}{\partial x}\left(G\frac{\partial \theta}{\partial t} - \beta G\frac{\partial^2 \theta}{\partial x^2} + H(G, \theta)\right) = 0. \tag{23}$$

where

$$F(S, G, \theta) = k_+(\theta)S - k_-(\theta)G \tag{24}$$

$$H(G, \theta) = G\theta + G\tau(\theta) - \pi(\theta). \tag{25}$$

The boundary conditions (12), (15) and (16) on a one-dimensional domain, $0 \leqslant x \leqslant L$, are

$$u(0, t) = u_0 \quad \text{(constant)}, \tag{26}$$

$$u(L, t) = u_L \quad \text{(constant)}, \tag{27}$$

$$\frac{\partial S}{\partial x} = 0 \quad \text{at } x = 0, L, \tag{28}$$

$$\frac{\partial G}{\partial x} = 0 \quad \text{at } x = 0, L, \tag{29}$$

yielding the conservation laws

$$\int_0^L \theta \, dx = u_L - u_0 = L\theta_0 \tag{30}$$

and

$$\int_0^L (S + G) \, dx = L(S_0 + G_0), \tag{31}$$

where the new, nondimensional steady state values are

$$S_0 = \frac{k_-(\theta_0)}{k_+(\theta_0)}, \quad G_0 = 1, \quad \theta_0 = (u_L - u_0)/L. \tag{32}$$

By integrating (23) we obtain

$$G\frac{\partial \theta}{\partial t} - \beta G\frac{\partial^2 \theta}{\partial x^2} + H(G, \theta) + \sigma(t) = 0, \tag{33}$$

where $\sigma(t)$ is the boundary stress. Thus, a constant boundary stress,

$$\sigma_0 = -H(G_0, \theta_0) \tag{34}$$

is exerted at the steady state.

Provided that $G \neq 0$, (33) gives

$$\int_0^L \left(\frac{\partial \theta}{\partial t} - \beta \frac{\partial^2 \theta}{\partial x^2} + (H(G, \theta) + \sigma(t))/G \right) dx = 0.$$

Application of the conditions (26)–(27), which fix u at the boundaries, gives

$$\left(\beta \frac{\partial \theta}{\partial x} \right)_0^L = \int_0^L (H(G, \theta) + \sigma(t))/G \, dx.$$

Thus, the boundary constraint for u is consistent with zero-gradient boundary conditions for θ, provided that

$$\int_0^L (H(G, \theta) + \sigma(t))/G \, dx = 0. \tag{35}$$

3 Linear analysis

We consider the behaviour of small perturbations of the state variables away from their steady state, (S_0, G_0, θ_0). Except when otherwise stated, we assume that β and D are positive parameters in (21)–(23). Linearisation of (21)–(23) yields a homogeneous system of equations describing the behaviour of these to small disturbances. A resulting solvability criterion relates the temporal and spatial components of the perturbations to the parameters in the model. This determines conditions on the parameters for when and how the steady state can become linearly unstable.

The linearised form of (21)–(23) is

$$\begin{pmatrix} \frac{\partial}{\partial t} - \frac{\partial^2}{\partial x^2} + k_+ & -k_- & \frac{k_-}{k_+}\frac{\partial}{\partial t} + F_\theta \\ -k_+ & \frac{\partial}{\partial t} - D\frac{\partial^2}{\partial x^2} + k_- & \frac{\partial}{\partial t} - F_\theta \\ 0 & H_G\frac{\partial}{\partial x} & \frac{\partial}{\partial x}\left(\frac{\partial}{\partial t} - \beta\frac{\partial^2}{\partial x^2} + H_\theta\right) \end{pmatrix} \begin{pmatrix} S - S_0 \\ G - G_0 \\ \theta - \theta_0 \end{pmatrix} = \mathbf{0}, \tag{36}$$

where

$$k_+ = k_-(\theta_0), \qquad F_\theta = \frac{\partial F}{\partial \theta}(S_0, G_0, \theta_0),$$

and similarly for k_-, H_G and H_θ.

We look for solutions to (36) of the form

$$S - S_0, \qquad G - G_0, \qquad \theta - \theta_0 \propto \exp(\sigma t + ikx). \tag{37}$$

Substitution into (36) yields a dispersion relation between σ and k^2 which must be satisfied if the system is to have a nontrivial solution. This is

$$k(\sigma^3 + A(k^2)\sigma^2 + B(k^2)\sigma + C(k^2)) = 0. \tag{38}$$

with

$$A(k^2) = A_1 k^2 + A_2, \tag{39}$$

$$B(k^2) = B_1 k^4 + B_2 k^2 + B_3, \tag{40}$$

$$C(k^2) = C_1 k^6 + C_2 k^4 + C_3 k^2 \tag{41}$$

and

$$A_1 = 1 + D + \beta, \qquad A_2 = k_+ + k_- + H_\theta - H_G,$$

$$B_1 = D + \beta(1 + D), \qquad B_2 = (1 + D)H_\theta + k_+(\beta + D) + k_-(\beta + 1) - H_G,$$

$$B_3 = (k_+ + k_-)H_\theta + (F_\theta - k_+ - k_-)H_G,$$

$$C_1 = D\beta, \qquad C_2 = DH_\theta + \beta(Dk_+ + k_-), \qquad C_3 = (Dk_+ + k_-)H_\theta + F_\theta H_G.$$

Our analysis earlier in this section indicates that the uniform steady state of (21)–(23) is stable to spatially uniform perturbations. To make the uniform steady state stable to perturbations with a spatial component, we require that the

roots of (38) have negative real parts for all positive k^2. If there is a root with a positive real part for some k^2, then the linear theory predicts that, provided the boundary conditions (28)–(30) are satisfied, small random perturbations away from the steady state can grow exponentially with a spatial wavelength of $2\pi/k$.

3.1 Conditions for real and Hopf bifurcations to spatial pattern

For biological pattern formation, we require that any spatial pattern bifurcations must have finite wave numbers, k, where $0 < k^2 < \infty$ and so

$$A_2 > 0, \qquad B_3 > 0, \qquad C_3 > 0. \tag{42}$$

In our subsequent analysis we assume that the solution domain is given by $0 \leqslant x \leqslant L$, $L = 2n\pi/k_c$, where k_c is the critical wave number at which the system bifurcates to linear instability

3.1.1 Real bifurcation. We consider the case where this bifurcation to linear instability occurs for the critical wave number, k_c, as an eigenvalue of the linear system passes through zero. In terms of the Routh Hurwitz conditions for stability, $A(k^2) > 0$ and $\Delta(k^2) = A(k^2)B(k^2) - C(k^2) > 0$ for all k, but

$$C(k^2)\begin{cases} = 0 & \text{if } k = k_c \\ > 0 & \text{if } k \neq k_c. \end{cases}$$

Thus we require

$$C_2 < 0 \tag{43}$$

and

$$C_2^2 - 4C_1C_3 = (DH_b - \beta(Dk_- + k_-))^2 - 4D\beta H_G F_\theta = 0, \tag{44}$$

giving the critical wave number, k_c, as

$$k_c^2 = -\frac{C_2}{2C_1}. \tag{45}$$

Constraint (43) requires that $H_\theta < 0$ (see σ-curve in Fig. 5) and therefore $F_\theta > 0$ so that $C_3 > 0$ (42). To meet (43), we choose the larger root for D in (44) as the critical value, D_c, at which $C(k_c^2)$ changes sign. As D increases through D_c, the maximum root for (38) will increase through zero. Linear analysis (37) predicts a corresponding bifurcation to the growth of unstable, stationary modes with wave number k_c.

3.1.2 Hopf bifurcation. We now consider the alternate case, given by pure imaginary bifurcation eigenvalues. In terms of the Routh Hurwitz criterion, $A(k^2) > 0$ and $C(k^2) > 0$ for all k, but

$$\Delta(k^2) = A(k^2)B(k^2) - C(k^2)\begin{cases} = 0 & \text{if } k = k_c \\ > 0 & \text{if } k \neq k_c. \end{cases}$$

We write

$$\Delta(k^2) = ak^6 + bk^4 + ck^2 + d.$$

where

$$a = A_1 B_1 - C_1 \geq 0,$$
$$b = A_1 B_2 + A_2 B_1 - C_2,$$
$$c = A_2 B_2 + A_1 B_3 - C_3,$$
$$d = A_2 B_3 > 0.$$

If we assume that long-range elastic effects and gel diffusion are insignificant ($\beta = D = 0$), then $a = 0$. In this case, the constraints

$$b > 0 \quad \text{and} \quad c < 0 \tag{46}$$

yield

$$k_c^2 = -\frac{c}{2b} \tag{47}$$

when

$$c^2 - 4bd = 0. \tag{48}$$

We assume (following Oster et al. 1985) that $\pi(\theta)$ is given by

$$\pi(\theta) = \pi_i(1 + \theta), \tag{49}$$

where π is constant denoting the magnitude of the osmotic stress. If $\theta_0 = 0$, then (25), (32) and (34) give

$$H_G = \pi(\theta_0) - \sigma_0 \tag{50}$$
$$H_V = H_\theta - H_G = 1 + \tau'(\theta_0) + \sigma_0. \tag{51}$$

Consequently

$$A(k^2) = k^2 + (k_+ + k_- + H_V), \tag{52}$$
$$B(k^2) = (H_V + k_-)k^2 + H_V(k_+ + k_-) + H_G F_\theta \tag{53}$$
$$C(k^2) = (k_- H_\theta + H_G F_\theta)k^2. \tag{54}$$

Provided $F_\theta \geq 0$, $H_G > 0$ and $H_V > 0$, the Routh–Hurwitz criterion is satisfied as $k^2 \to 0^+, \infty$.

Our simplifications means that the condition for a Hopf bifurcation (48) can be written as a quadratic polynomial in $\pi(\theta_0)$, namely

$$a_1(\pi - \sigma_0)^2 + b_1(\pi - \sigma_0) + c_1 = 0, \tag{55}$$

where

$$a_1 = k_-^2,$$
$$b_1 = -2k_-(H_V^2 + 2(k_- + k_-)H_V + k_-(k_+ + k_-)) - 4(H_V + k_-)(H_V + k_+ + k_-)F_\theta,$$
$$c_1 = (H_V^2 + 2(k_+ + k_-)H_V + k_-(k_- + k_-))^2 - 4(H_V + k_-)(H_V + k_- + k_-)(k_+ + k_-)H_V.$$

To satisfy (46), we choose the larger root for π in (55) as the critical value, π_c, at which $A(k^2)$ changes sign, producing a pair of pure imaginary roots for (38), given by $\sigma_c = \pm i\omega_c$, where

$$\omega_c = +\sqrt{B(k_c^2)|_{\pi = \pi_c}} \tag{56}$$

Thus (37) predicts a corresponding bifurcation to the exponential growth of linearly unstable, dispersive modes, with wave speed a_c and wave number k_c, given from (47) by

$$k_c^2 = \frac{k_+(\pi_c - k_+ - k_-) - H_V(H_V + 2k_- + 2k_+)}{2(H_V + k_-)}. \tag{57}$$

4 Nonlinear analysis

4.1 Motivation and theory

Linear analysis indicates that for critical parameter sets spatial patterns may arise as the homogeneous steady state becomes linearly unstable with wavelength $2\pi/k_c$. This is only valid for small time and infinitesimal perturbations; over a longer time scale the exponential growth predicted by linear analysis is dominated by nonlinear terms. We now include nonlinear terms that can bound the growth of the perturbations so that they evolve to a new heterogeneous steady state solution. Associated with this process are three relevant time regions. The first, denoted by t, is the initial time range in which the solution begins to develop from the initial perturbation. Here we expect the linear theory to be valid. The second region, where time is denoted by T, is that in which the nonlinear effects begin to become important. This is followed by the third region, which is reached as T becomes infinite.

We use a standard method for the nonlinear analysis (see, for example, Matkowski 1970) and consider the case where the bifurcation to spatial pattern occurs as an eigenvalue of the linear system passes through zero (see Sect. 3.1.1). In Sect. 4.5 we show that for the alternate case, given by a Hopf bifurcation, the analysis can be reduced to an appropriate form by a change of variables.

4.2 Analysis of stationary pattern formation

We analyse here the nonlinear behaviour of exponentially growing spatially stationary modes, predicted by linear analysis (Sect. 3.1.1) as occurring when the maximum eigenvalue for (38) increases through zero. Provided (42)–(43) are satisfied, this bifurcation to linearly unstable modes happens when D increases through D_c, the larger root of (44). The resulting wavelength of the growing pattern is $2\pi/k_c$, where k_c is given by (45). For the purpose of this analysis, we assume that the domain length is an integral multiple of the wavelength; in other words $L = 2n\pi/k_c$: there is no practical loss of generality.

We make an ϵ^2 perturbation away from the critical value for D,

$$D = D_c + \epsilon^2 \nu \quad \text{where } 0 < \epsilon \ll 1 \text{ and } \nu = \pm 1, \tag{58}$$

and use this as the basis for a series expansion of σ,

$$\sigma(k_c^2, D) = \sigma(k_c^2, D_c) + \frac{\partial \sigma}{\partial D}(k_c^2, D_c)\epsilon^2 \nu + \mathcal{O}(\epsilon^4). \tag{59}$$

The $\mathcal{O}(\epsilon^2)$ term in (59) can be calculated from (38) as

$$\frac{\partial \sigma}{\partial D}(k_c^2, D_c) = \frac{-\partial C/\partial D(k_c^2)}{B(k_c^2)|_{D=D_c}}, \tag{60}$$

where $B(k^2)$ is given in (40), and (41) gives

$$\partial C/\partial D(k_c^2) = \beta k_c^6 + (H_\theta + \beta k_-)k_c^4 + k_+ H_\theta k_c^2. \tag{61}$$

Introduction of a slow time scale, $T = \epsilon^2 t$, means that exponential growth terms, predicted by the linear analysis (37), can be written as $a(T)\exp(\pm ik_c x)$, where

$$a(T) = \exp\left(\frac{\partial \sigma}{\partial D}(k_c^2, D_c)\nu T\right) \tag{62}$$

and $\partial\sigma/\partial D(k_c^2, D_c)$ is given in (60).

To simplify the analysis, we set $F_{\theta\theta} = 0$. This would be the case if, for example, we took piecewise linear dynamics for $k_+(\theta)$ and $k_-(\theta)$ (see Fig. 4). While retaining the essential nonlinear behaviour, this reduces the terms to a manageable number.

With the new expressions for D in (58) and T, we use (21)–(23) to write a vector equation for the perturbed system:

$$\boldsymbol{L}\begin{pmatrix} S - S_0 \\ G - G_0 \\ \theta - \theta_0 \end{pmatrix} + \boldsymbol{N} + \boldsymbol{E} = \boldsymbol{0}, \tag{63}$$

where

$$\boldsymbol{L} = \begin{pmatrix} -\dfrac{\partial^2}{\partial x^2} + k_- & -k_- & F_\theta \\ -k_+ & -D_c\dfrac{\partial^2}{\partial x^2} + k_- & -F_\theta \\ 0 & H_G\dfrac{\partial}{\partial x} & \dfrac{\partial}{\partial x}\left(-\beta\dfrac{\partial^2}{\partial x^2} + H_\theta\right) \end{pmatrix}, \tag{64}$$

$$\boldsymbol{N} = \begin{pmatrix} F_{S\theta}(S - S_0)(\theta - \theta_0) + F_{G\theta}(G - G_0)(\theta - \theta_0) \\ -F_{S\theta}(S - S_0)(\theta - \theta_0) - F_{G\theta}(G - G_0)(\theta - \theta_0) \\ \dfrac{\partial}{\partial x}\left(-\beta(G - G_0)\dfrac{\partial^2}{\partial x^2}(\theta - \theta_0) + H_{G\theta}(G - G_0)(\theta - \theta_0)\right. \\ \quad + H_{\theta\theta}(\theta - \theta_0)^2/2 + H_{G\theta\theta}(G - G_0)(\theta - \theta_0)^2/2 \\ \quad \left. + H_{\theta\theta\theta}(\theta - \theta_0)^3/6\right) \end{pmatrix} + \text{h.o.t.}, \tag{65}$$

$$\boldsymbol{E} = \epsilon^2\begin{pmatrix} \dfrac{\partial}{\partial T}(S - S_0) + \dfrac{\partial}{\partial T}(\theta - \theta_0)k_-/k_+ \\ \dfrac{\partial}{\partial T}(G - G_0) + \dfrac{\partial}{\partial T}(\theta - \theta_0) - \nu\dfrac{\partial^2}{\partial x^2}(G - G_0) \\ \dfrac{\partial}{\partial x}\dfrac{\partial}{\partial T}(\theta - \theta_0) \end{pmatrix} + \text{h.o.t.}, \tag{66}$$

$$H_G = \frac{\partial H}{\partial G}(S_0, G_0, \theta_0),$$

H_0, $F_{S\theta}$, $F_{G\theta}$, $H_{G\theta}$, $H_{\theta\theta}$, $H_{G\theta\theta}$ and $H_{\theta\theta\theta}$ are defined in a similar way to H_G, and h.o.t. indicates higher order terms.

We assume an asymptotic representation for S, G and θ, given by

$$S = S_0 + \sum_{j=1} \epsilon^j S_j(x, T), \quad G = G_0 + \sum_{j=1} \epsilon^j G_j(x, T), \quad \theta = \theta_0 + \sum_{j=1} \epsilon^j \theta_j(x, T). \tag{67}$$

Our asymptotic expansions for S, G and θ (67) reduce the analysis of the nonlinear system (63) to a hierarchy of linear equations for increasing powers of ϵ (see Appendix A). The first such equation is

$$\boldsymbol{L}\begin{pmatrix} S_1 \\ G_1 \\ \theta_1 \end{pmatrix} = \mathbf{0}, \tag{68}$$

while the equation for the jth power of ϵ is

$$\boldsymbol{L}\begin{pmatrix} S_j \\ G_j \\ \theta_j \end{pmatrix} + \boldsymbol{N}_j + \boldsymbol{E}_j = \mathbf{0}, \tag{69}$$

where $\boldsymbol{N}_j$ and $\boldsymbol{E}_j$ are calculated from the terms $S_{j-1}, G_{j-1}, \theta_{j-1}, \ldots, S_1, G_1, \theta_1$. Since (68) possesses non-trivial solutions, a necessary and sufficient condition for a solution to (69) is given by the orthogonality relation

$$\lim_{T\to\infty} \frac{1}{T} \int_0^T \int_0^{2\pi/k_c} (S^*, G^*, \theta^*) \cdot \overline{(\boldsymbol{N}_j + \boldsymbol{E}_j)}\, dx\, dT = 0, \tag{70}$$

where $(S^*, G^*, \theta^*)^t$ is a bounded solution of the adjoint problem

$$\boldsymbol{L}^*\begin{pmatrix} S^* \\ G^* \\ \theta^* \end{pmatrix} = \mathbf{0}$$

and $\boldsymbol{L}^*$ is the adjoint of $\boldsymbol{L}$. This relation, given by the Fredholm Alternative, suppresses secular terms which arise if solutions to (68) are present in $\boldsymbol{N}_j + \boldsymbol{E}_j$.

Application of (70) to the hierarchy linear equations indicates that no secular terms arise in the first two powers of ϵ (Appendix A). At $\mathcal{O}(\epsilon^3)$ the orthogonality constraint (70) yields a Landau equation for the maximum amplitude, $|\alpha|$, of θ_1 (see Appendix A, Eqs. (100) and (111)).

The boundary conditions for (21)–(23), given by (26) (29), constrain α to be real. Therefore, provided $\nu = +1$ and $Y > 0$ (see Appendix A, Eq. (113)), the Landau equation predicts that the large time solution evolves to

$$\begin{aligned} S &= k_+ + \epsilon(X/Y)^{1/2} u_1 \cos(k_c x) + \mathcal{O}(\epsilon^2), \\ G &= 1 + \epsilon(X/Y)^{1/2} u_2 \cos(k_c x) + \mathcal{O}(\epsilon^2), \\ \theta &= (u_L - u_0)/L + \epsilon(X/Y)^{1/2} \cos(k_c x) + \mathcal{O}(\epsilon^2), \end{aligned} \tag{71}$$

where u_1, u_2, X and Y are given in Appendix A by (101) and (102), (112) and (113), respectively.

4.3 *Pattern space and sensitivity analysis for stationary pattern formation*

We now consider the pattern space (equivalent to a *Turing* space (Murray 1982)) of parameters needed for stationary pattern formation and the sensitivity of this pattern space to small changes in the model parameters. When parameters lie within the pattern space we expect that the spatially homogeneous steady state will bifurcate to a stable pattern formation through the growth of linearly unstable modes. We choose representative forms for $F(S, G, \theta)$ (Fig. 7) and $H(G, \theta)$ (Fig. 8) and consider the resulting projection of the pattern space on to D-β space.

As suggested in the previous section, the dynamics for $k_-(\theta)$ and $k_-(\theta)$ are piecewise linear (Fig. 7). Based on Oster et al. (1985), we choose $\tau(\theta)$ and $\pi(\theta)$ as

$$\tau(\theta) = \frac{\tau}{1 - (\theta + \tau_1)^2} \tag{72}$$

$$\pi(\theta) = \frac{\pi}{1 + \theta}. \tag{73}$$

Here τ and π are constants denoting the magnitudes of the $\tau(\theta)$ and $\pi(\theta)$ respectively and $-\tau_1$ is the dilation at which the contractile elements are strongest. If, for example, $\tau = 4$, $\pi = 3$, and $\tau_1 = -0.1$, then $H_\theta(G_0, \theta_0) < 0$ when $\theta_0 = 1$ (Fig. 8), and thus the constraint $C_2 < 0$ is met (43).

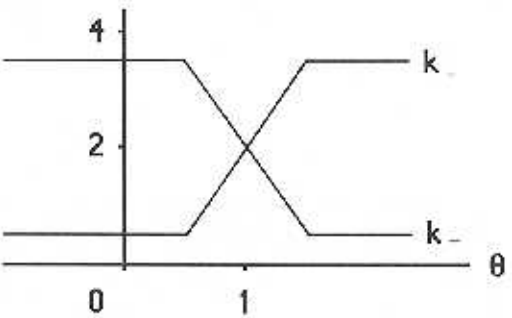

Fig. 7. Piecewise linear dynamics for k_+ and k_-. The sol-gel dynamics, given by $F(S, G, \theta) = k_+(\theta)S - k_-(\theta)G$ (see (24)), yield $F_{S\theta} = F_{G\theta} = 3$ for $1/2 \leq \theta \leq 3/2$ and $F_{S\theta} = F_{G\theta} = 0$ elsewhere

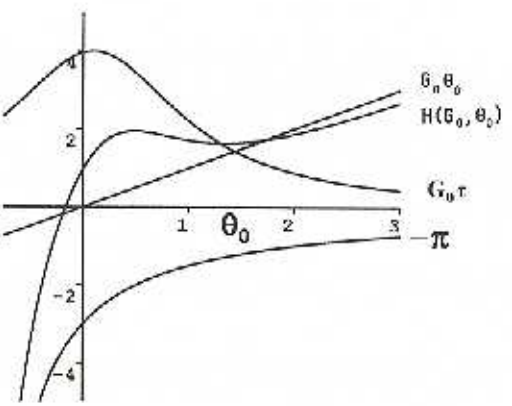

Fig. 8. Steady state dynamics for $H(G_0, \theta_0)$. The steady state dynamics for $H(G_0, \theta_0)$ are $H(G_0, \theta_0) = G_0\theta_0 - G_0\tau(\theta_0) - \pi(\theta_0)$ (25), where $\tau(\theta_0)$ and $\pi(\theta_0)$ are given by (72) and (73) respectively. Parameter values are $\tau = 4$, $\pi = 3$ and $\tau_1 = -0.1$

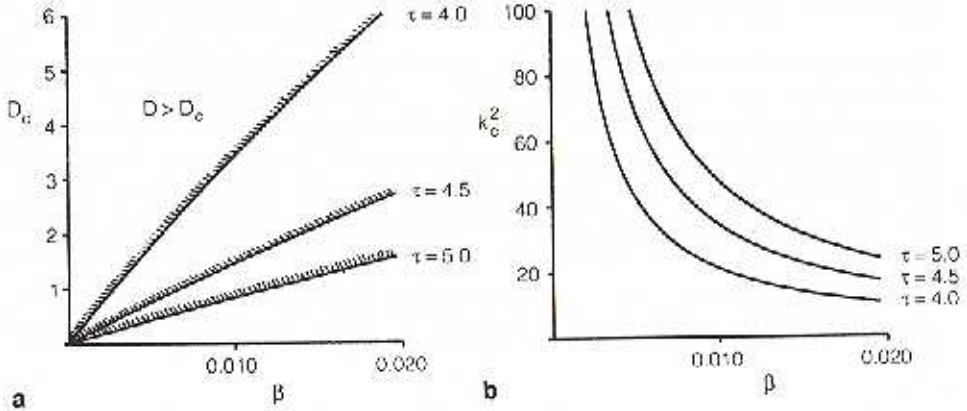

Fig. 9a,b. β-D Pattern space and resulting critical wave number. **a** The pattern space is given by $D > D_c$, where $D = D_c$ is the solution to (44). **b** The resulting critical wave number, $\pm k_c$, is the solution to (45). We observe that as τ increases, D_c decreases and k_c^2 increases. Parameter values are $\pi = 3$ and $\tau_1 = -0.1$

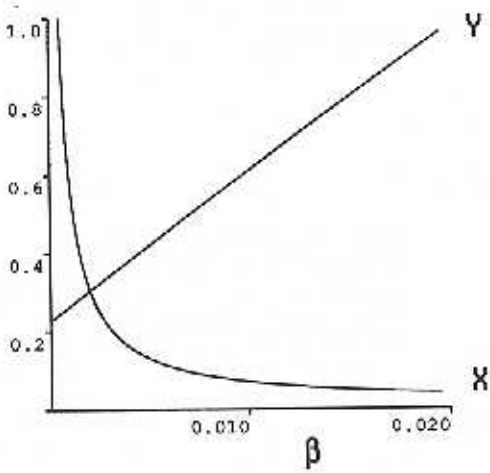

Fig. 10. β-dependencies for the Landau constants, X and Y. The Landau constants, X and Y, are calculated from (112) and (113)

Equations (44) and (45) yield the D-β pattern space and the resulting critical wave number, $\pm k_c$ (Fig. 9(a) and (b)). The β-dependencies for the Landau constraints, X and Y, calculated from (112) and (113), are shown in Fig. 10.

Figure 11 shows the critical dispersion relation between $\max_{1 \le i \le 3} \Re(\sigma_i)$ and k^2 defined by the cubic (38), when $\beta = 0.01$ and D is given by (44). All other parameter values are as given in this section. The resulting critical parameters and solution constants are:

$$D_c = 3.435,\ k_c = 4.593,\ X = 0.07071,\ Y = 0.6077,\ a_1 = -0.2534,\ a_2 = 0.07376 \tag{74}$$

(see Figs. 9 and 10 and Eqs. (101) and (102)). The resulting boundary stress is given by (34) as $\sigma_0 = -1.71$.

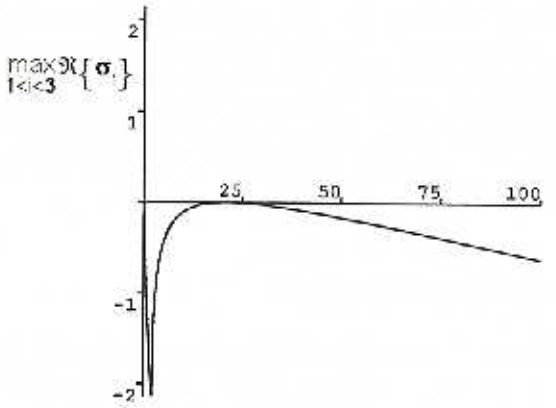

Fig. 11. Critical dispersion relation leading to spatial pattern formation. The dispersion relation is shown for $\beta = 0.01$ and $D = D_c = 3.435$. Parameter values are $\tau = 4$, $\pi = 3$ and $\tau_1 = -0.1$. For supercritical D there is a bifurcation to spatial pattern as $\max_{1<l<3} \Re(\sigma_l)$ becomes positive

Table 1. Sensitivity coefficients for stationary pattern formation. Rows refer to critical parameters and solution constants and columns refer to changes in model parameters. The entries in the table are dimensionless sensitivity coefficients, evaluated at the values given in (74). For example, the entry in the top, left corner is $\partial D_c / \partial \beta$

	$\partial/\partial\beta$	$\partial/\partial\pi$	$\partial/\partial\tau$	$\partial/\partial\tau_1$	$\partial/\partial F_{S0}$	$\partial/\partial F_{G0}$
D_c	3.13×10^{2}	3.72×10^{0}	-7.56×10^{0}	2.63×10^{1}	5.87×10^{-1}	5.81×10^{-1}
k_c	-2.39×10^{1}	1.32×10^{0}	2.92×10^{0}	-1.03×10^{1}	5.41×10^{-3}	5.41×10^{-3}
X	-6.04×10^{0}	-1.16×10^{-1}	2.42×10^{-1}	-8.43×10^{-1}	-1.26×10^{-2}	-1.26×10^{-2}
Y	3.76×10^{1}	1.77×10^{-1}	7.32×10^{-1}	-1.92×10^{2}	2.33×10^{-1}	1.15×10^{-2}
u_1	-2.42×10^{1}	-1.37×10^{-1}	3.01×10^{-1}	-1.05×10^{0}	-4.27×10^{-2}	-4.27×10^{-3}
u_2	3.19×10^{-1}	-3.99×10^{-2}	7.48×10^{0}	-2.57×10^{-1}	-1.55×10^{-4}	-1.55×10^{-4}

Using Eqs. (44), (45), (101), (102), (112) and (113), we numerically calculated the sensitivity of the critical parameters (D_c and k_c) and solution constants (X, Y, u_1 and u_2), given in (74), to small changes in the following model parameters: β (long-range elasticity), π (osmotic stress, see (73)), τ and τ_1 (contractile stress, see (72)) and F_{S0} and F_{G0} (dynamics of sol-gel phase change, see (24) and Fig. 7). Results are shown in Table 1. Rows refer to the critical parameters and solution constants and columns refer to the changes in model parameters. Thus each entry in Table 1 indicates the sensitivity of a critical parameter or solution constant to changes in a model parameter. The fact that the original equations and parameters (21) (25) are nondimensionalised means that the numbers in Table 1 are dimensionless sensitivity coefficients.

Observing the columns in Table 1, we note that the critical parameters and solution constants are very robust to changes in the sol-gel dynamics (entries in the columns labelled $\partial/\partial F_{S0}$ and $\partial/\partial F_{G0}$ are all less than unity). This insensitivity suggests that our qualitative formulation of the 'solation-contraction' hypothesis in Sect. 2.2 is justifiable, because a more exact formulation would make very little change to the constants in (74) which define the solution (71). Table 1 indicates that the critical parameters and solution constants are fairly robust to changes in the magnitudes of the osmotic and contractile stresses (entries in the

columns labelled $\partial/\partial\pi$ and $\partial/\partial\tau$ are order 1), but are sensitive to changes in the long-range elasticity and to the value of τ_1 (some entries in the columns labeled $\partial/\partial\beta$ and $\partial/\partial\tau_1$ are much larger than unity). The sensitivity to β and τ_1 suggests the biological importance of these parameters; thus experimental investigations into the nature of the long-range interactions in cytogel (β) and into the exact form of the dilation-dependent actomyosin contractility (τ_1) may aid to further understand the patterns.

4.4 *Numerical simulation of stationary pattern formation*

In the last section, we saw that when the critical gel-diffusion constant, D_c, is exceeded ($D > D_c$), a spatial pattern of wavelength $2\pi/k_c$, arises. Provided that $\epsilon = (D - D_c)^{1/2}$ is sufficiently small, this spatial pattern is shown to exist as a stable configuration when the Landau constant Y is positive (71). A comparison between this analytical result and numerical simulations (method outlined below) indicates agreement for the D_c given in (74) and similar large time steady state solutions for small ϵ. However, we anticipate that (71) may still give an indication of the resulting pattern in the biologically relevant situation where ϵ is not necessarily a very small parameter. To this end, we numerically solve (21)–(23), with zero-gradient boundary conditions for S, G and θ, using the parameters given in the previous section and $D = 4.0$ (Fig. 12). So as to be able to apply a Crank–Nicholson type finite difference solution method we integrate (23) (see (33)) and determine $\sigma(t)$ from (35) at every time step. Thus u remains fixed at the boundaries and (26)–(27) are met. The value of $\sigma(t)$ remained very close to that of σ_0 (34) throughout the simulation.

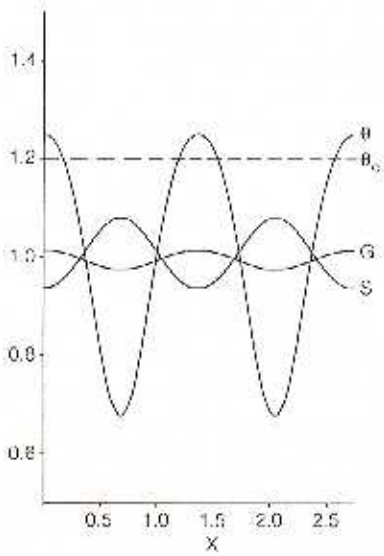

Fig. 12. Numerical solution for stationary pattern in the sol-gel model. Shown is the large time ($t = 2000$), finite difference numerical solution of the model Eqs. (21)–(23). The domain size is given by $0 \leq x \leq 4\pi/k_c$, where k_c, the model parameters, and a discussion of the numerical method are given in the text (Sects. 4.3–4.4). Boundary conditions are zero-gradient, and initial conditions are given by small (< 0.001) random perturbations of S, G and θ about their steady states. When the dilation (θ) increases above a critical level, θ_c, bundling proteins bind the actin fibres, thereby reinforcing the already dense actin meshwork in regions of high gel concentration

4.5 Analysis of dispersive wave pattern formation

In this section we analyse the nonlinear behaviour of dispersive waves. Linear analysis (Sect. 3.1.2) predicts a bifurcation to these exponentially growing, dispersive waves as the maximum eigenvalues for (38) increase through $\sigma = \sigma_i = +i\sigma_c$.

We consider the simplified case, given by $\beta = D = 0$, in the interest of keeping the problem analytically tractable. Thus the bifurcation to linearly unstable modes happens as π increases through π_c, the larger root of (55). The resulting wavelength of the growing dispersive waves is $2\pi/k_c$, where k_c is given by (57).

Since the system bifurcates to spatial pattern at $\sigma_i = \pm i\sigma_c$, with a wave number $k_i = \pm k_c$, linear theory suggests that we look for solutions to (21)–(23) (with $\beta = D = 0$) which can be expressed in terms of the moving coordinate system:

$$z_1^* = x + \frac{\sigma_c}{k_c} t, \qquad z_2^* = x - \frac{\sigma_c}{k_c} t, \quad t^* = t.$$

Assuming that solutions are of the form $S(z_1^*, z_2^*, t^*)$, $G(z_1^*, z_2^*, t^*)$ and $\theta(z_1^*, z_2^*, t^*)$ and proceeding by analogy with the method of multiple scales, we require that S, G, and θ satisfy

$$0 = \left(\frac{\partial}{\partial t^*} + \frac{\sigma_c}{k_c}\left(\frac{\partial}{\partial z_1^*} - \frac{\partial}{\partial z_2^*}\right)\right)S + \left(\frac{\partial}{\partial z_1^*} + \frac{\partial}{\partial z_2^*}\right)\left(S\left(\frac{\partial}{\partial t^*} + \frac{\sigma_c}{k_c}\left(\frac{\partial}{\partial z_1^*} - \frac{\partial}{\partial z_2^*}\right)\right)u\right) - \left(\frac{\partial}{\partial z_1^*} + \frac{\partial}{\partial z_2^*}\right)^2 S + F(S, G, \theta), \tag{75}$$

$$0 = \left(\frac{\partial}{\partial t^*} + \frac{\sigma_c}{k_c}\left(\frac{\partial}{\partial z_1^*} - \frac{\partial}{\partial z_2^*}\right)\right)G + \left(\frac{\partial}{\partial z_1^*} + \frac{\partial}{\partial z_2^*}\right)\left(G\left(\frac{\partial}{\partial t^*} + \frac{\sigma_c}{k_c}\left(\frac{\partial}{\partial z_1^*} - \frac{\partial}{\partial z_2^*}\right)\right)u\right) - F(S, G, \theta), \tag{76}$$

$$0 = \left(\frac{\partial}{\partial z_1^*} + \frac{\partial}{\partial z_2^*}\right)\left(G\left(\frac{\partial}{\partial t^*} + \frac{\sigma_c}{k_c}\left(\frac{\partial}{\partial z_1^*} - \frac{\partial}{\partial z_2^*}\right)\right)\theta + H(G, \theta)\right). \tag{77}$$

Here, the time and space derivatives have been re-written as

$$\frac{\partial}{\partial t} \to \frac{\partial}{\partial t^*} + \frac{\sigma_c}{k_c}\left(\frac{\partial}{\partial z_1^*} - \frac{\partial}{\partial z_2^*}\right)$$

$$\frac{\partial}{\partial x} \to \frac{\partial}{\partial z_1^*} + \frac{\partial}{\partial z_2^*}.$$

In the interest of notational simplicity, we now dispense with the asterisks when referring to the moving coordinate system.

Small perturbations about the uniform steady state are expressed as

$$S^* = S - S_0, \qquad G^* = G - G_0, \qquad \theta^* = \theta - \theta_0.$$

Dropping asterisks, we look for solutions of the form

$$S, G, \theta \propto \exp(\sigma t + ikx) = \gamma \exp(\sigma_1 t + ikz_1) + (1-\gamma)\exp(\sigma_2 t + ikz_2), \quad (78)$$

where $0 \leqslant \gamma \leqslant 1$ and

$$\sigma_1 = \sigma - i\frac{k}{k_c}\sigma_c, \qquad \sigma_2 = \sigma + i\frac{k}{k_c}\sigma_c.$$

Bifurcation to spatial pattern takes place when $\sigma_1(k^2, \pi_c) = \sigma_2(k^2, \pi_c) = 0$. The fact that this bifurcation occurs at zero eigenvalues allows us to apply the nonlinear bifurcation theory discussed in Sect. 4.2. The value of γ is determined by the boundary conditions (see Appendix B).

We make an ϵ^2 perturbation away from the critical value for π,

$$\pi = \pi_c + \epsilon^2 \nu \quad \text{where } 0 < \epsilon \ll 1 \text{ and } \nu = \pm 1, \quad (79)$$

and use this as the basis for series expansions of σ_1 and σ_2:

$$\sigma_i(k_c^2, \pi) = \sigma_i(k_c^2, \pi_c) + \frac{\partial \sigma_i}{\partial \pi}(k_c^2, \pi_c)\epsilon^2 \nu + \mathcal{O}(\epsilon^4), \quad i = 1, 2. \quad (80)$$

The $\mathcal{O}(\epsilon^2)$ terms in (80) can be calculated from (38) as

$$\frac{\partial \sigma_1}{\partial \pi}(k_c^2, \pi_c) = \left(\frac{\partial C}{\partial \pi}(k_c^2) + i\sigma_c \frac{\partial B}{\partial \pi}(k_c^2)\right)\Big/ (2(B(k_c^2) - i\sqrt{A(k_c^2)C(k_c^2)})|_{\pi=\pi_c}) \quad (81)$$

and

$$\frac{\partial \sigma_2}{\partial \pi}(k_c^2, \pi_c) = \overline{\frac{\partial \sigma_1}{\partial \pi}(k_c^2, \pi_c)},$$

where $A(k^2)$, $B(k^2)$ and $C(k^2)$ are given in (52)–(54),

$$\frac{\partial B}{\partial \pi}(k^2) = F_\theta \quad \text{and} \quad \frac{\partial C}{\partial \pi}(k^2) = (k_\theta + F_\theta)k^2. \quad (82)$$

Introduction of a slow time scale, $T = \epsilon^2 t$, means that exponential growth terms, predicted by the linear analysis (78), can be written as $a(T)\exp(ik_c z_1)$, $a(T)\exp(-ik_c z_1)$, $\bar{a}(T)\exp(ik_c z_2)$ and $\bar{a}(T)\exp(-ik_c z_2)$, where

$$a(T) = \exp\left(\frac{\partial \sigma_1}{\partial \pi}(k_c^2, \pi_c)\nu T\right) \quad (83)$$

and $\partial\sigma_1/\partial\pi(k_c^2, \pi_c)$ is as given in (81).

As in our analysis for stationary pattern formation, we set $F_{\theta\theta} = 0$, so as to reduce the terms to a manageable number while retaining the essential nonlinear behaviour. With the new expressions for π (79) and T, we use (75)–(77) to write a vector equation for the perturbed system:

$$\boldsymbol{L}\begin{pmatrix} S \\ G \\ 0 \end{pmatrix} + \boldsymbol{N} + \boldsymbol{E} = \boldsymbol{0}, \quad (84)$$

where

$$\boldsymbol{L} = \begin{bmatrix} \dfrac{\sigma_c}{k_c}\left(\dfrac{\partial}{\partial z_1} - \dfrac{\partial}{\partial z_2}\right) & -k_- & \dfrac{\sigma_c}{k_c}\dfrac{k_-}{k_-}\left(\dfrac{\partial}{\partial z_1} - \dfrac{\partial}{\partial z_2}\right) + F_0 \\ -\left(\dfrac{\partial}{\partial z_1} + \dfrac{\partial}{\partial z_2}\right)^2 + k_+ & & \\ -k_+ & \dfrac{\sigma_c}{k_c}\left(\dfrac{\partial}{\partial z_1} - \dfrac{\partial}{\partial z_2}\right) + k_- & \dfrac{\sigma_c}{k_c}\left(\dfrac{\partial}{\partial z_1} - \dfrac{\partial}{\partial z_2}\right) - F_0 \\ 0 & \left(\dfrac{\partial}{\partial z_1} + \dfrac{\partial}{\partial z_2}\right) H_G & \left(\dfrac{\partial}{\partial z_1} + \dfrac{\partial}{\partial z_2}\right) \\ & & \left(\dfrac{\sigma_c}{k_c}\left(\dfrac{\partial}{\partial z_1} - \dfrac{\partial}{\partial z_2}\right) + H_\theta\right) \end{bmatrix}, \tag{85}$$

$$\boldsymbol{N} = \begin{bmatrix} \dfrac{\sigma_c}{k_c}\left(S\left(\dfrac{\partial}{\partial z_1} - \dfrac{\partial}{\partial z_2}\right)\theta + \left(\dfrac{\partial}{\partial z_1} + \dfrac{\partial}{\partial z_2}\right)S \cdot \left(\dfrac{\partial}{\partial z_1} - \dfrac{\partial}{\partial z_2}\right)\int \theta\, dx\right) \\ + F_{S\theta}S\theta + F_{G\theta}G\theta \\ \dfrac{\sigma_c}{k_c}\left(G\left(\dfrac{\partial}{\partial z_1} - \dfrac{\partial}{\partial z_2}\right)\theta + \left(\dfrac{\partial}{\partial z_1} + \dfrac{\partial}{\partial z_2}\right)G \cdot \left(\dfrac{\partial}{\partial z_1} - \dfrac{\partial}{\partial z_2}\right)\int \theta\, dx\right) \\ - F_{S\theta}S\theta - F_{G\theta}G\theta \\ \left(\dfrac{\partial}{\partial z_1} + \dfrac{\partial}{\partial z_2}\right)\left(\dfrac{\sigma_c}{k_c}G\left(\dfrac{\partial}{\partial z_1} - \dfrac{\partial}{\partial z_2}\right)\theta\right. \\ \left. + H_{G\theta}G\theta + H_{\theta\theta}\theta^2/2 + H_{G\theta\theta}G\theta^2/2 + H_{\theta\theta\theta}\theta^3/6\right) \end{bmatrix} + \text{h.o.t.}, \tag{86}$$

$$\boldsymbol{E} = c^2 \begin{bmatrix} \dfrac{\partial S}{\partial T} + \dfrac{\partial \theta}{\partial T}k_-/k_+ \\ \dfrac{\partial G}{\partial T} + \dfrac{\partial \theta}{\partial T} \\ \left(\dfrac{\partial}{\partial z_1} + \dfrac{\partial}{\partial z_2}\right)\left(\dfrac{\partial \theta}{\partial T} + v(G + \theta)\right) \end{bmatrix} + \text{h.o.t.}, \tag{87}$$

$$H_G = \frac{\partial H}{\partial G}(S_0, G_0, \theta_0)\Big|_{a = a_c},$$

and H_0, F_{S0}, $F_{G\theta}$, $H_{G\theta}$, $H_{\theta\theta}$, $H_{G\theta\theta}$ and $H_{\theta\theta\theta}$ are defined in a similar way to H_G.

We assume an asymptotic representation for S, G and θ, given by

$$S = S_0 + \sum_{j=1} c^j S_j(z_1, z_2, T), \qquad G = G_0 + \sum_{j=1} c^j G_j(z_1, z_2, T),$$

$$\theta = \theta_0 + \sum_{j=1} c^j \theta_j(z_1, z_2, T). \tag{88}$$

Substitution into (84) results in a hierarchy of linear equations which are evaluated for increasing powers of ε. Using similar analysis to that described for stationary wave patterns (Sect. 4.2), we arrive at a Landau equation for the maximum amplitude, $|\alpha|$, of θ_1 (see Appendix B, Eqs. (116) and (128)). A bounded stable solution of this equation requires that $\nu = 1$ and $Y > 0$ (see Appendix B, Eq. (130)) and predicts the maximum amplitude of θ_1 as $|\alpha| = (X/Y)^{1/2}$. Thus as $T \to \infty$ we expect α to lie on a circle in the complex plane which is centred about the origin and has a radius of $(X/Y)^{1/2}$.

We denote the real and imaginary parts of α by $\alpha = \alpha_r + i\alpha_i$. Ordinary differential equations, showing the T-dependencies for α_r and α_i, arise from considering the real and imaginary parts in Eq. (126) in Appendix B. As $T \to \infty$, these equations are

$$\frac{\partial \alpha_r}{\partial T} = \phi \alpha_i \tag{89}$$

$$\frac{\partial \alpha_i}{\partial T} = -\phi \alpha_r, \tag{90}$$

where ϕ, given in terms of components calculated in Appendix B, is

$$\phi = \nu \frac{\Im\left(\dfrac{\boldsymbol{R}^{(3)} \cdot \overline{\boldsymbol{W}^{(1)}}}{\boldsymbol{R}^{(1)} \cdot \overline{\boldsymbol{W}^{(1)}}}\right)}{\Re\left(\dfrac{\boldsymbol{R}^{(3)} \cdot \overline{\boldsymbol{W}^{(1)}}}{\boldsymbol{R}^{(1)} \cdot \overline{\boldsymbol{W}^{(1)}}}\right)}. \tag{91}$$

The solution to (89)–(90) is

$$\begin{pmatrix} \alpha_r \\ \alpha_i \end{pmatrix} = \begin{pmatrix} A_1 \sin(\phi T) + A_2 \cos(\phi T) \\ -A_2 \sin(\phi T) + A_1 \cos(\phi T) \end{pmatrix}, \tag{92}$$

where the coefficients A_1 and A_2 satisfy $A_1^2 + A_2^2 = |\alpha|^2 = X/Y$.

By choosing

$$A_1 = |\alpha| \cos(\eta)$$
$$A_2 = |\alpha| \sin(\eta),$$

the solution (92) can be re-written as

$$\begin{pmatrix} \alpha_r \\ \alpha_i \end{pmatrix} = |\alpha| \begin{pmatrix} \sin(\phi T + \eta) \\ \cos(\phi T + \eta) \end{pmatrix}. \tag{93}$$

Thus α slowly moves about the circle in the complex plane, which is centred at the origin and has a radius of $(X/Y)^{1/2}$ with a period of $2\pi/\phi T$ (Fig. 13).

Without loss of generality we choose a zero phase shift by setting $\eta = 0$; the qualitative, large time behaviour of (93) is not affected by a shift in phase. Thus Eqs. (89) and (90) and Eq. (128) in Appendix B predict that the large time solution evolves to

$$\begin{aligned} S = k_- / k_- + 2\varepsilon (X/Y)^{1/2} & ((u_{1r} \sin(\phi T) - u_{1i} \cos(\phi T)) \cos(k_c z_1) \\ & - (u_{1i} \sin(\phi T) + u_{1r} \cos(\phi T)) \sin(k_c z_1) \\ & + (u_{1r} \sin(\phi T) - u_{1i} \cos(\phi T)) \cos(k_c z_2) \\ & + (u_{1i} \sin(\phi T) + u_{1r} \cos(\phi T)) \sin(k_c z_2)) + \mathcal{O}(\varepsilon^2) \end{aligned} \tag{94}$$

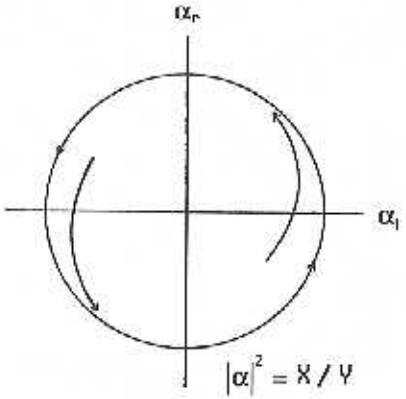

Fig. 13. Movement of α about the complex plane. As $T \to \infty$, α moves about the circle in the complex plane, which is centred at the origin and has a radius of $(X/Y)^{1/2}$

$$G = 1 + 2\varepsilon(X/Y)^{1/2}((u_{2r}\sin(\phi T) - u_{2i}\cos(\phi T))\cos(k_c z_1) - (u_{2r}\sin(\phi T) + u_{2i}\cos(\phi T))\sin(k_c z_1) + (u_{2r}\sin(\phi T) - u_{2i}\cos(\phi T))\cos(k_c z_2) + (u_{2r}\sin(\phi T) + u_{2i}\cos(\phi T))\sin(k_c z_2)) + \mathcal{O}(\varepsilon^2) \quad (95)$$

$$0 = 2\varepsilon(X/Y)^{1/2}(\sin(\phi T)\cos(k_c z_1) + \cos(\phi T)\cos(k_c z_1) + \sin(\phi T)\cos(k_c z_2) + \cos(\phi T)\cos(k_c z_2)) + \mathcal{O}(\varepsilon^2), \quad (96)$$

where u_{1r}, u_{1i}, u_{2r} and u_{2i} are the real and imaginary parts of u_1 and u_2 given in Appendix B by (117) and (118), and X and Y are given in Appendix B by (129) and (130) respectively.

4.6 Pattern space and sensitivity analysis for dispersive wave pattern formation

We now consider the space of parameters needed for dispersive wave pattern formation and the sensitivity of this pattern space to small changes in the model parameters. When parameters lie within the pattern space we expect that the spatially homogeneous steady state will bifurcate to a stable dispersive wave pattern through the growth of linearly unstable modes.

As suggested in Sect. 3.1.2, we choose $\pi(\theta)$ as given by (49) and $\theta_0 = 0$. Piecewise linear dynamics for $k_+(\theta)$ and $k_-(\theta)$ yield $F_0 = 0$ (see Fig. 7). The values of $k_+(\theta_0)$ and $k_-(\theta_0)$ are chosen to be 0.75 and 1.25 respectively.

Choosing $\tau(\theta)$ to be given by (72), with $\tau_1 = 0$, yields

$$H_V = 1 + \sigma_0 \quad (97)$$

by Eq. (51). Thus H_V is independent of $\tau(\theta_0)$. Equations (34) and (50) yield

$$H_G = \pi - \sigma_0 = \tau. \quad (98)$$

In other words, as there are no elastic stresses, the osmotic stress must exactly balance the traction and boundary stresses in order for the system to stay at the $\theta = 0$ steady state.

Having fixed the steady state dynamics for $F(S_0, G_0, \theta_0)$ and the forms for $\tau(\theta)$ and $\pi(\theta)$, we now consider the resulting projection of the pattern space on

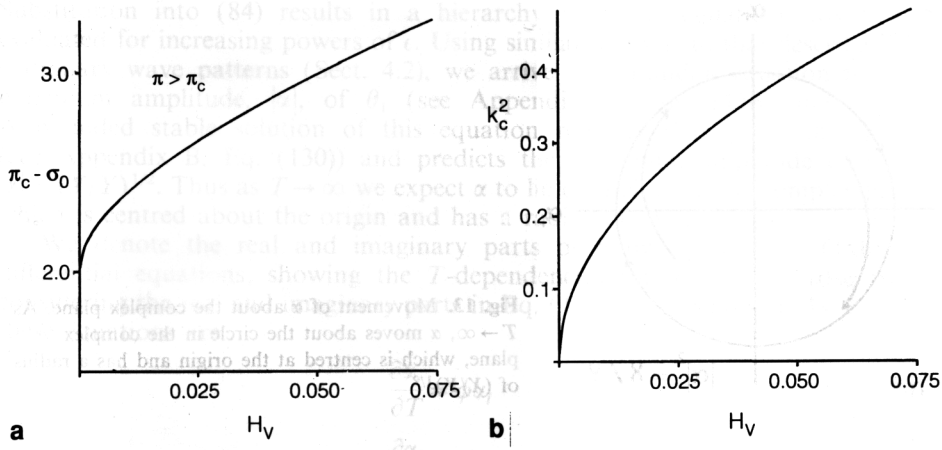

Fig. 14a,b. H_V-π Pattern space and resulting critical wave number. **a** The pattern space is given by $\pi > \pi_c$, where $\pi = \pi_c$ is the solution to (55). **b** The resulting critical wave number, $\pm k_c$, is the solution to (57)

to π-H_V space. The boundary of this space is given by Eq. (55). At this boundary, the resulting critical wave number, $\pm k_c$, is given by (57) (Fig. 14(a) and (b)). The H_V-dependencies for the Landau constants, X and Y, and for the periodicity constant, ϕ, calculated from (91), (129) and (130), are shown in Fig. 15.

The critical dispersion relation between σ and k^2 is defined by the cubic (38). The resulting critical parameters and solution constants for $H_V = 0.06$ are

$$\pi_c = 2.165, \quad k_c = 0.65591, \quad \sigma_c = 0.8301, \quad X = 0.03944, \quad Y = 1.445,$$
$$\phi = 0.1458, \quad u_{1r} = -1.403, \quad u_{1i} = -0.4669, \quad u_{2r} = -1.019, \quad u_{2i} = -0.2673 \tag{99}$$

(see Figs. 14 and 15 and Eqs. (55)–(56) and (117)–(118)). Equations (97) and (98) yield $\sigma_0 = -0.94$ and $\tau = 3.105$ as the corresponding boundary stress and traction parameter. Our choice of $\theta_0 = 0$ means that $H_G > 0$ and $H_V > 0$ and thus the Routh–Hurwitz criterion for stability is satisfied as $k^2 \to 0, \infty$ (see Sect. 3.1.2).

Using Eqs. (55), (56), (57), (91), (117), (118), (129) and (130), we numerically calculated the sensitivity of the critical parameters (π_c and k_c) and solution constants (X, Y, ϕ, u_{1r}, u_{1i}, u_{2r} and u_{2i}), given in (99), to small changes in H_V (see (97)) and F_S and F_G (see (24) and Fig. 7). Results are shown in Table 2. Rows refer to the critical parameters and solution constants and the columns refer to changes in model parameters. Thus each entry in Table 2 indicates the sensitivity of a critical parameter or solution constant to changes in a model parameter. The fact that the original equations and parameters (21)–(25) are nondimensionalised means that the numbers in Table 2 are dimensionless sensitivity coefficients.

Observing the columns in Table 2, we note that the critical parameters and solution constants are fairly robust to changes in the sol-gel dynamics (entries in the columns labeled $\partial/\partial F_S$ and $\partial/\partial F_G$ are typically order 1 or smaller), but are

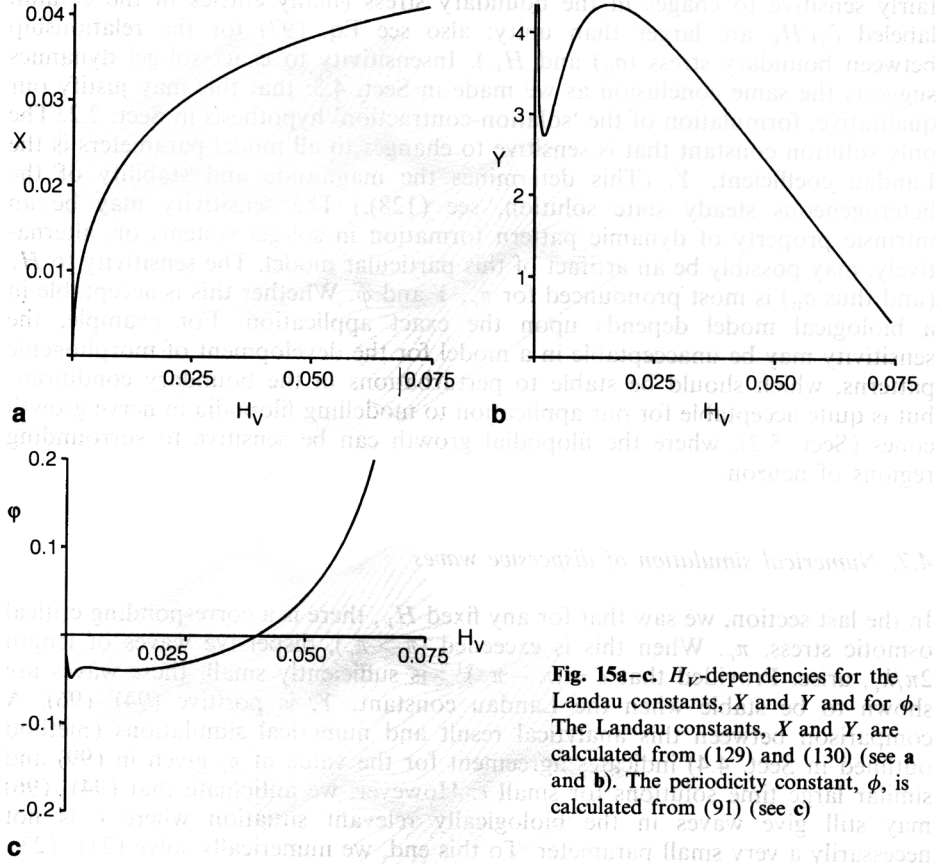

Fig. 15a–c. H_V-dependencies for the Landau constants, X and Y and for ϕ. The Landau constants, X and Y, are calculated from (129) and (130) (see **a** and **b**). The periodicity constant, ϕ, is calculated from (91) (see **c**)

Table 2. Sensitivity coefficients for dynamic pattern formation. Rows refer to critical parameters and solution constants and columns refer to changes in model parameters. The entries in the table are dimensionless sensitivity coefficients, evaluated at the values given in (99). For example, the entry in the top, left corner is $\partial\pi_c/\partial H_V$

	$\partial/\partial H_V$	$\partial/\partial F_S$	$\partial/\partial F_G$
π_c	1.24×10^{1}	1.54×10^{0}	-1.01×10^{0}
k_c	2.70×10^{0}	1.62×10^{-1}	-3.66×10^{-2}
σ_c	4.27×10^{0}	2.05×10^{-1}	-3.34×10^{-1}
X	1.52×10^{-1}	-1.70×10^{-2}	-3.02×10^{-3}
Y	-7.59×10^{1}	2.61×10^{1}	7.06×10^{0}
ϕ	1.32×10^{1}	-3.95×10^{0}	-1.16×10^{0}
u_{1r}	1.54×10^{0}	1.88×10^{0}	1.21×10^{0}
u_{1i}	-1.04×10^{0}	7.39×10^{-1}	3.94×10^{-1}
u_{2r}	-2.50×10^{-1}	-9.54×10^{-3}	-5.96×10^{-3}
u_{2i}	-3.90×10^{-1}	6.71×10^{-2}	2.12×10^{-2}

fairly sensitive to chages in the boundary stress (many entries in the column labeled $\partial/\partial H_V$ are larger than unity; also see Eq. (97) for the relationship between boundary stress (σ_0) and H_V). Insensitivity to exact sol-gel dynamics suggests the same conclusion as we made in Sect. 4.3: that this may justify our qualitative, formulation of the 'solation-contraction' hypothesis in Sect. 2.2. The only solution constant that is sensitive to changes to all model parameters is the Landau coefficient, Y. (This determines the magnitude and stability of the heterogeneous steady state solution, see (128).) The sensitivity may be an intrinsic property of dynamic pattern formation in sol-gel systems or, alternatively, may possibly be an artifact of this particular model. The sensitivity to H_V (and thus σ_0) is most pronounced for π_c, Y and ϕ. Whether this is acceptable in a biological model depends upon the exact application. For example, the sensitivity may be unacceptable in a model for the development of morphogenic patterns, which should be stable to perturbations in the boundary conditions, but is quite acceptable for our application to modelling filopodia in nerve growth cones (Sect. 5.2), where the filopodial growth can be sensitive to surrounding regions of neuron.

4.7. Numerical simulation of dispersive waves

In the last section, we saw that for any fixed H_V, there is a corresponding critical osmotic stress, π_c. When this is exceeded ($\pi > \pi_c$), dispersive waves of length $2\pi/k_c$, arise. Provided that $\epsilon = (\pi - \pi_c)^{1/2}$ is sufficiently small, these waves are shown to be stable when the Landau constant, Y, is positive (94)–(96). A comparison between this analytical result and numerical simulations (method outlined in Sect. 4.4) indicates agreement for the value of π_c given in (99) and similar large time solutions for small ϵ. However, we anticipate that (94)–(96) may still give waves in the biologically relevant situation where ϵ is not necessarily a very small parameter. To this end, we numerically solve (21)–(23), with zero-gradient boundary conditions for S, G and θ, using the parameters given in the previous section, except $\pi = 2.365$ and $\tau = 3.305$ (see (98)) (Fig. 16). The numerical solution method is described in Sect. 4.4.

5 Applications to biological pattern formation

Our model for sol-gel dynamics (21)–(23) predicts that distinct spatial (Sects. 4.2–4.4) and spatio-temporal (Sects. 4.5–4.7) patterns will spontaneously arise when the model parameters lie within the appropriate *parameter* space for pattern formation. In this section we use these results to suggest how actin-dense patterns arise from the contractile cytogel cortex of certain cells.

Actin-dense patterns typically take the form of fibre bundles, whether protruding from the cell surface as stationary structures (for example, microvilli and stereocilia) or as dynamic structures (for example, microspikes and filopodia). The fibre bundles arise, to a large extent, from the action of actin-binding proteins, such as those shown in Fig. 1 whose activity is usually related to pH or calcium levels. Because calcium levels and dilation are negatively correlated (Sect. 2.2) and that pH levels frequently follow calcium levels (Oster et al. 1985) we assume that both the calcium and pH levels decrease with dilation. Even with this simplifying assumption, the behaviours of actin-binding proteins are very

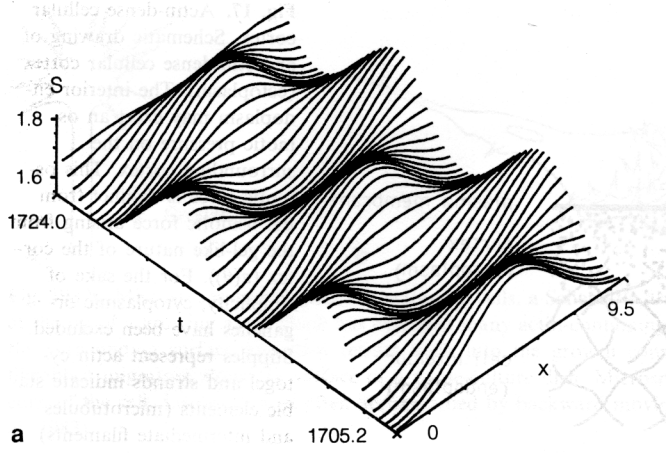

a

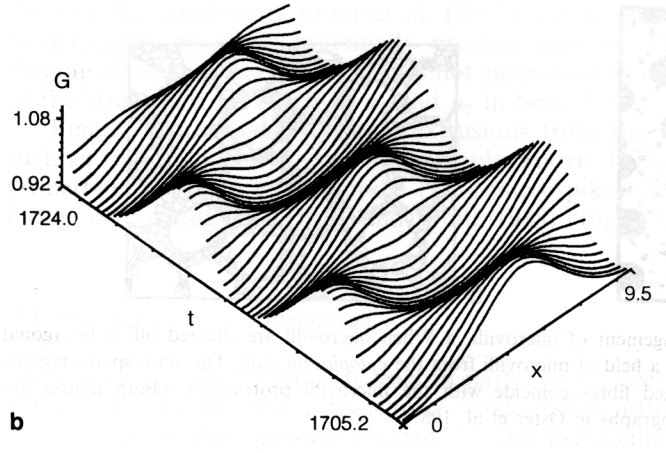

b

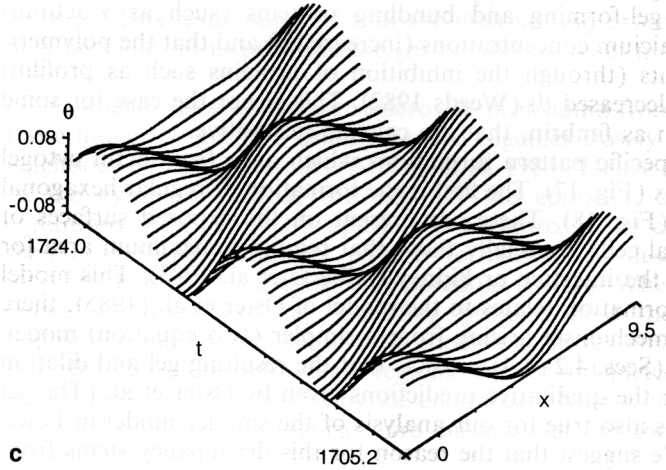

c

Fig. 16a–c. Numerical solution for dispersive waves in the sol-gel model. Shown is the large time finite difference numerical solution of the model Eqs. (21)–(23) for sol **a**, gel **b** and dilation **c**. The domain size is given by $0 \leqslant x \leqslant 2\pi/k_c$, where k_c, the model parameters, and a discussion of the numerical method are given in the text (Sects. 4.6–4.7). Boundary conditions are zero-gradient, and initial conditions are given by small (<0.001) random perturbations of S, G and θ about their steady states

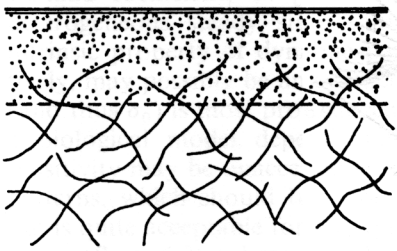

Fig. 17. Actin-dense cellular cortex. Schematic drawing of an actin-dense cellular cortex (ectoplasm). The interior endoplasm may exert an osmotic pressure on the surrounding cortex. This osmotic force is distinct from the osmotic force arising from the gel-like nature of the cortex ($\pi(\theta)$). For the sake of simplicity, cytoplasmic organelles have been excluded. Stipples represent actin cytogel and strands indicate stable elements (microtubules and intermediate filaments)

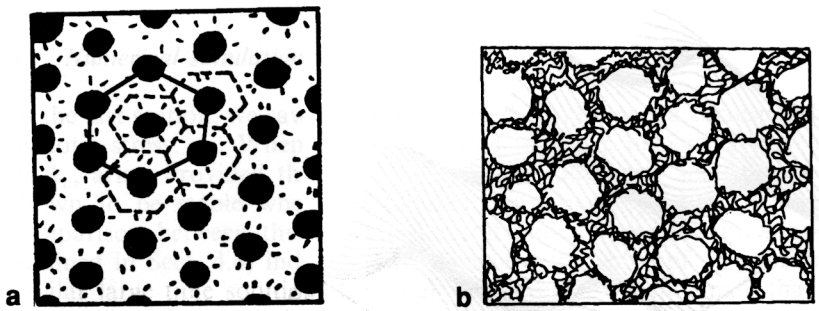

Fig. 18a,b. Hexagonal arrangement of microvilli. **a** When microvilli are sheared off, a hexagonal pattern is evident. **b** View of a field of microvilli from the *cytoplasmic* side. The actin-sparse regions between the bands of aligned fibres coincide with the microvilli protrusions. (Both figures are redrawn from electron micrographs in Oster et al. 1985)

complex (see, for example, Weeds 1982). As a general rule, however, we expect that calcium-sensitive gel-forming and bundling proteins (such as α-actinin) become active at low calcium concentrations (increased θ) and that the polymerisation of actin filaments (through the inhibition of proteins such as profilin) occurs at a high pH (decreased θ) (Weeds 1982). This is not the case for some bundling proteins, such as fimbrin, that are calcium-insensitive.

We consider two specific pattern formations which arise from actin cytogel present in the cell cortex (Fig. 17). The first is the formation of regular hexagonal patterns of microvilli (Fig. 18). These are present on the exposed surfaces of many kinds of epithelial cells, especially those that require a maximum area for absorption, such as in the intestine or kidney (Alberts et al. 1983). This model for microvilli pattern formation relates to the model of Oster et al. (1985); there the authors suggest a mechanism arising from a simpler (two equation) model. However, our analysis (Secs. 4.2–4.4) predicts that the resulting gel and dilation fluctuations differ from the qualitative predictions given by Oster et al. (The gel is out of phase.) This is also true for our analysis of the simpler model in Lewis and Murray (1991). We suggest that the reason for this discrepancy stems from

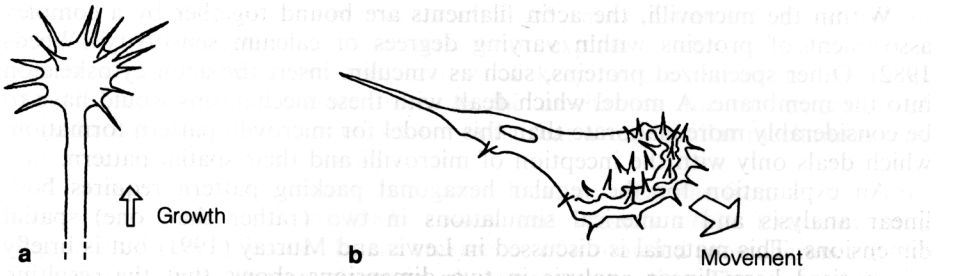

Fig. 19a,b. Microspikes and filopodia in actin-rich cells. **a** Schematic drawing of a nerve growth cone at the tip of a growing axon which has extended many actin-containing filopodia. These extend onto the surrounding surface and then retract back into the growth cone. **b** Schematic drawing of a fibroblast migrating along the surface of a tissue-culture dish. Microspikes extend from the leading edge of the cell. Locomotion is often accompanied by backward moving "ruffles". (After Alberts et al. 1983)

the fact that analysis in Oster et al. (1985) was restricted to showing that the model equations could potentially produce pattern. The resulting qualitative diagram (Fig. 4, Oster et al. 1985) is not supported by calculations for the phase of the strain and gel (such as u_1 and u_2 in Sect. 4.3).

Finally, we consider dynamic extrusions from the actin cortex. Structures such as ruffles and blebs (see, for example, Harris 1973) as well as microspikes (Alberts et al. 1983) and filopodia (long microspikes) are found in a variety of motile or growing cells (Bray and White 1988) (Fig. 19).

5.1 Microvilli pattern formation

Microvilli protrusions arise, at least in part, from a pressure difference between the endoplasm and the extracellular fluid. Tilney (1975) shows this clearly; an increase in the pressure exerted by the extracellular fluid results in the disappearance of the microvilli, while a subsequent decrease to the normal extracellular pressure results in the reappearance of microvilli after about 30 minutes. This result suggests that the internal and external pressure differences may be sufficient to protrude the cortex into incipient microvilli (see Oster et al. 1985).

Epithelial cells which have microvilli protruding from their surface (such as those lining the gut) are usually packed together closely and are bound to each neighbour by tight junctions (Alberts et al. 1983). Hence we expect no movement of the cytoplasm across the edge of the epithelial cell and the boundary conditions (12), (15), (16) apply. Furthermore, if the cells are packed tightly, then $\sigma_0 < 0$ and stationary pattern formation (as described in Sect. 4.3) is possible. Figure 12 illustrates this potential pattern. When the dilation increases above a critical level, σ_c, bundling proteins bind the actin fibres, thereby reinforcing the already dense actin meshwork in regions of high gel concentration. Between these actin-dense regions, the gel is depleted and less able to resist the osmotic pressure exerted by the endoplasm. Microvilli ultimately result when the weakened areas of cortex are pushed out by the endoplasmic osmotic pressure.

Within the microvilli, the actin filaments are bound together by a complex assortment of proteins within varying degrees of calcium sensitivity (Weeds 1982). Other specialized proteins, such as vinculin, insert the actin cytoskeleton into the membrane. A model which dealt with these mechanisms would have to be considerably more elaborate than this model for microvilli pattern formation, which deals only with the inception of microvilli and their spatial pattern.

An explanation for the regular hexagonal packing pattern requires both linear analysis and numerical simulations in two (rather than one) spatial dimensions. This material is discussed in Lewis and Murray (1991) but is briefly summarised here: linear analysis in two dimensions shows that the resulting patterns have a geometric periodicity. Thus we expect that patterns such as squares, rhombi or hexagons may occur. Of these, the hexagonal pattern has a high degree of structural stability and thus is most likely to occur. Alternately, if we suppose that the foci of contraction form sequentially from an initiation site, each new row will form in the space between the previous foci, thereby leading to a hexagonally symmetric pattern (see, for example, Murray 1989).

Structural, developmental and organizational similarities between microvilli and stereocilia suggest the possibility of common formative mechanisms (Oster et al. 1985). The internal structure of stereocilia is like that of large microvilli (Tilney and De Rosier 1986; Alberts et al. 1983). Stereocilia, found on the surface of the inner ear, are instrumental in converting sound waves into electrical impulses. They protrude from the cuticular plate of specialised hair cells in an array of hexagonal patterns (Hudspeth 1983). This array arises from a field of small regularly spaced nodes which later grow into rods, each of which is filled with aligned actin fibres (Oster et al. 1985). The possibility that stereocilia arise as osmotically generated protrusions from the actin cortex could be tested by the application of an extracellular osmotic force during development. A resulting reversal of development would indicate that such a hypothesis is valid.

5.2 Dynamic pattern formation: Microspikes and filopodia

Structural and functional resemblances between the protrusive cellular processes present in a variety of motile cells led Tosney and Wessels (1983) to suggest that the filopodia and microspikes, which extend from nerve growth cones and fibroblasts, may arise from analogous mechanical and chemical origins.

While the nerve growth cone is the growing tip of an axon, fibroblasts are motile embryonic cells which secrete a fibrous material, helping to make up an extracellular matrix within which cells move. In both cells, the microspikes and filopodia may guide the movement of the cells up haptotactic gradients (Alberts et al. 1983); protrusions adhering to the substrate contract and move the cell towards the adhesive site.

Both fibroblasts and growth cones have actin-rich, gel-like, contractile cortices (Dunn 1980; Tosney and Wessels 1983). For each cell, forward movement is approximately 0.01 μm/s (Alberts et al. 1983; Harris 1973; Abercrombie et al. 1970); however, the movement mechanisms are quite different. In the case of the nerve growth cone, forward movement results from the growth of the axon (Fig. 19) (Alberts et al. 1983). Movement of fibroblasts, on the other hand, is thought to arise from opposing flows of gel in the cell cortex and of sol in the endoplasm (Bray and White 1988; cf. Oster 1984). These flows may be considerably faster

than the movement of the fibroblast itself (0.05 μm/s) (Dunn 1980) and add an extra level of complexity to any model for explaining the extension of microspikes in fibroblasts. In the interest of keeping the model as simple as possible, we choose to concentrate on the mechanism for the extension of filopodia in nerve growth cones, while noting that a very similar mechanism may also be applicable to fibroblasts.

Filopodia emerge at seemingly random locations near the front of the nerve growth cone (Alberts et al. 1983; Tosney and Wessels 1983). Extrusion of a filopodium is often preceded by the emergence of a rounded protruberance at the cell margin, which appears dense in phase-contrast optics. This protruberance forms over the course of 2 to 5 seconds before losing its dense appearance as the filopodium emerges (Argiro et al. 1985). Extrusion of the filopodium is rapid, initial extension rates being of the order of 0.1 μm/s (Argiro et al. 1985).

Current theory (Argiro et al. 1985; Tosney and Wessels 1983) suggests that extrusion may occur by a rapid polymerisation of actin, in a manner consistent with models for extension of the acrosomal process of sperm (see, for example, Tilney and Inoué 1982). Here, rapid assembly of the actin polymers which make up the acrosomal process can be triggered by a rise in pH. It is likely that a profilin-like protein (see Fig. 1) stabilises the pool of actin monomers which serves as a source for the polymer growth (Weeds 1982). This extrusion mechanism contrasts with that suggested for microvilli (Sect. 5.1) where the endoplasmic pressure plays a key role.

After 30 to 150 seconds the filopodia reach a length of approximately 5 μm and typically are reabsorbed or retreat back into the growth cone. Some filopodia which adhere to the substratum may remain stable for longer time periods (Argiro et al. 1985). Filopodial formations cease when the nerve growth cone is treated with cytochlasin, a drug which prevents the sol-gel transition by binding to the actin filaments (Forscher and Smith 1988).

Tosney and Wessels (1983) suggest that for a growth cone the transition from a smooth surface to a protrusion may require alterations in the interactions between actin and myosin-like proteins, or alterations in the gel-sol condition of the cytoplasm. Using results from our mechanochemical model (21)–(23) (Sects. 4.6–4.7), we will show that such spatial and temporal changes in the dilation (θ) and the sol (S) and gel (G) concentrations may indeed occur in a manner consistent with the extrusion of filopodia.

Experimental measurements clearly indicate that filopodial extrusions correlate with local 'hotspots' in intracellular calcium levels (Conner 1986; Cohan et al. 1987; Kater et al. 1988; Silver et al. 1990). However, the fact that the diffusion rate of calcium occurs on a much faster time scale than that of the filopodial extrusion suggests that the calcium gradients must result from significant local differences in either the intracellular release/resequestering rates or the cell membrane permeability to calcium (Conner 1986; Cohan et al. 1987; Silver et al. 1990). Thus the biochemical nature of calcium regulation in the neuronal cytoskeleton becomes important for understanding the localized calcium 'hotspots' and their relation to filopodial extrusions.

Calcium regulation in the neuronal cytoskeleton is extremely complex and is an ongoing area of research (see Forscher 1989, for example). As well as regulating sol-gel dynamics through intermediate proteins (see Fig. 2), calcium levels can themselves be regulated by the intermediate proteins. However, it is likely that the polymerisation-promoting protein, polyphosphatidylinositol 4,5-bisphophate (PIP_2), that inhibits profilin (see Fig. 1), plays a key role in the

formation of filopodia. The rapid actin polymerisation which occurs during filopodial extrusion may be regulated by an interaction between PIP_2 and the fragmentation protein, gelsolin. Gelsolin creates a pool of monomers (sol) by fragmenting the actin, while PIP_2 promotes the rapid actin polymerisation (see Forscher 1989 for the biochemical details). However, PIP_2 also controls local calcium levels; hydrolysis of PIP_2 eventually produces two messenger products: protein kinase C (PKC) and inositol 1,4,5-triphosphate (IP_3) which in turn regulate the influx of calcium across the cell membrane and facilitate the release of intracellular calcium. Lastly, these increased calcium levels can activate the gelsolin to fragment more actin.

We suggest that a possible mechanism for the growth of a filopodium is the following: when the sol-gel cortex contracts below a critical dilation, θ_c, and the sol concentration increases, activated gelsolin interacts with PIP_2 so as to trigger growth of the filopodium. The PIP_2 may also be instrumental in controlling local calcium levels (and thus the pH) during the growth of the filopodium. The dense, rounded protruberance observed by Argiro et al. (1985) as preceding the filopodial extrusion may be a contracted nodule of gel. A subsequent change in cytogel dilation, arising from oscillatory behaviour (shown in Sects. 4.6–4.7) (Fig. 20), could sufficiently alter the PIP_2-gelsolin interaction to reverse the polymerization process and result in the withdrawal of the filopodia. Thus a possible mechanochemical mechanism for the inception of filopodia can be formulated by using only the inherent properties of the cytogel cortex.

Other biochemical pathways to filopodial growth may be possible. For example, the neurone-specific growth associated protein, GAP-43 (alias B-50, F-1, pp46 or p57) induces filopodia in non-neuronal cells (Zuber et al. 1989). But this does not demonstrate that the molecule is essential for filopodial formation since many cell types extend filopodia but do not contain GAP-43, including

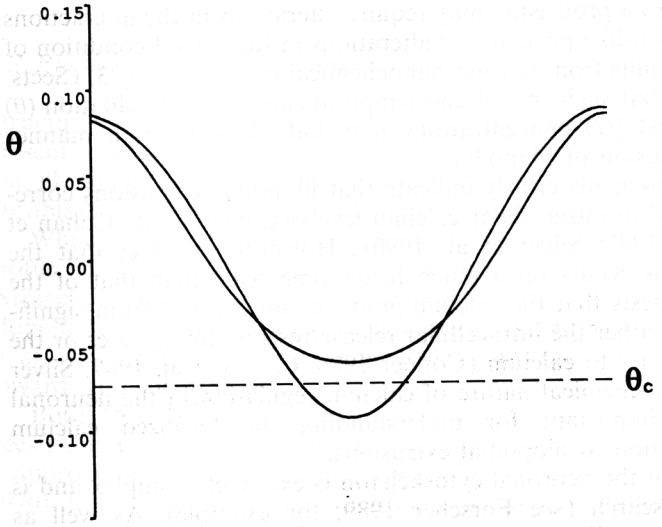

Fig. 20. Simulation of possible dynamics leading to a filopodial extrusion and retraction. When the dilation decreases below the critical level, θ_c, rapid assembly of the actin polymers results in the growth of a filopodium. This process is reversed when the dilation increases above θ_c. The time-dependent profile for θ is taken from Fig. 16 for $t = 1706$ (lower) and $t = 1707$ (upper)

dendritic growth cones (Gordon-Weeks 1989). However, regardless of the exact biochemical pathway taken for filopodial growth, we suggest that the dynamic mechanochemical instabilities, arising from sol-gel interactions in the growth cone cortex, may provide a spatial patterning of perturbations which then give rise to filopodia.

Appendix A: Nonlinear analysis of stationary pattern formation

Substitution of (67) into (63) results in a hierarchy of linear equations for increasing powers of ϵ. Through solving these equations for the first three powers of ϵ we calculate the coefficients, X and Y, of the Landau equation (111).

We define the matrix L_k as arising from the action of $\boldsymbol{L}$ on terms of the form $\exp(ikx)$. Thus

$$L_k = \begin{pmatrix} k^2 + k_+ & -k_- & F_\theta \\ -k_+ & D_c k^2 + k_- & -F_\theta \\ 0 & ikH_G & ik(\beta k^2 + H_\theta) \end{pmatrix}.$$

At $\mathcal{O}(\epsilon)$ we have

$$\boldsymbol{L}\begin{pmatrix} S_1 \\ G_1 \\ \theta_1 \end{pmatrix} = \boldsymbol{0}.$$

Therefore, solutions are of the form

$$\begin{pmatrix} S_1 \\ G_1 \\ \theta_1 \end{pmatrix} = \alpha \boldsymbol{U} \exp(ik_c x) + \bar{\alpha}\bar{\boldsymbol{U}} \exp(-ik_c x) \tag{100}$$

where $\alpha = \alpha_0 a(T)$ and

$$\boldsymbol{U} = \begin{pmatrix} u_1 \\ u_2 \\ 1 \end{pmatrix}$$

is the eigenvector given by $L_{k_c}\boldsymbol{U} = \boldsymbol{0}$. Thus

$$u_1 = -((D_c k_c^2 + k_-)(\beta k_c^2 + H_\theta) + F_\theta H_G)/(k_+ H_G) \tag{101}$$

$$u_2 = -(\beta k_c^2 + H_\theta)/H_G. \tag{102}$$

At $\mathcal{O}(\epsilon^2)$ we have

$$\boldsymbol{L}\begin{pmatrix} S_2 \\ G_2 \\ \theta_2 \end{pmatrix} + \boldsymbol{N}_2 = \boldsymbol{0},$$

where

$$N_2 = \begin{pmatrix} F_{S\theta}S_1\theta_1 + F_{G\theta}G_1\theta_1 \\ -F_{S\theta}S_1\theta_1 - F_{G\theta}G_1\theta_1 \\ \dfrac{\partial}{\partial x}\left(-\beta G_1 \dfrac{\partial^2\theta_1}{\partial x^2} + H_{G\theta}G_1\theta_1 + H_{\theta\theta}\theta_1^2/2\right) \end{pmatrix}$$

$$= \boldsymbol{Q}^{(1)}\alpha^2 \exp(2ik_c x) + \overline{\boldsymbol{Q}^{(1)}}\bar{\alpha}^2 \exp(-2ik_c x) + \boldsymbol{Q}^{(2)}|\alpha|^2,$$

for

$$\boldsymbol{Q}^{(1)} = \begin{pmatrix} q_1^{(1)} \\ q_2^{(1)} \\ 2ik_c q_3^{(1)} \end{pmatrix} \quad \text{and} \quad \boldsymbol{Q}^{(2)} = \begin{pmatrix} q_1^{(2)} \\ q_2^{(2)} \\ 0 \end{pmatrix},$$

with components

$$q_1^{(1)} = u_1 F_{S\theta} + u_2 F_{G\theta},$$

$$q_2^{(1)} = -q_1^{(1)},$$

$$q_3^{(1)} = u_2(\beta k_c^2 + H_{G\theta}) + H_{\theta\theta}/2$$

$$q_1^{(2)} = 2u_1 F_{S\theta} + 2u_2 F_{G\theta},$$

$$q_2^{(2)} = -q_1^{(2)}.$$

Thus

$$\begin{pmatrix} S_2 \\ G_2 \\ \theta_2 \end{pmatrix} = \alpha_1 \boldsymbol{U} \exp(ik_c x) + \bar{\alpha}_1 \bar{\boldsymbol{U}} \exp(-ik_c x$$

$$+ \boldsymbol{V}^{(1)}\alpha^2 \exp(2ik_c x) + \bar{\boldsymbol{V}}^{(1)}\bar{\alpha}^2 \exp(-2ik_c x) + \boldsymbol{V}^{(2)}|\alpha|^2,$$

where

$$L_{2k_c}\boldsymbol{V}^{(1)} + \boldsymbol{Q}^{(1)} = \boldsymbol{0} \tag{103}$$

$$L_0 \boldsymbol{V}^{(2)} + \boldsymbol{Q}^{(2)} = \boldsymbol{0}. \tag{104}$$

Solving (103) for $\boldsymbol{V}^{(1)}$ yields

$$v_1^{(1)} = -D_c v_2^{(1)}$$

$$v_3^{(1)} = (q_2^{(1)} + D_c(k_+ + k_- + 4k_c^2)v_2^{(1)})/F_\theta,$$

$$v_2^{(1)} = -\frac{q_3^{(1)}F_\theta + (4\beta k_c^2 + H_\theta)q_2^{(1)}}{H_G F_\theta + D_c(4\beta k_c^2 + H_\theta)(k_+ + k_- + 4k_c^2)}.$$

Implicit in our asymptotic representations (67) are the assumptions that S_j, G_j and θ_j are $\mathcal{O}(1)$ for all $j \geqslant 0$, and thus that $\boldsymbol{V}^{(1)}$ is also $\mathcal{O}(1)$. Hence our analysis is restricted to those parameter spaces in which the denominator of $v_2^{(1)}$ remains $\mathcal{O}(1)$.

The matrix L_0 is rank deficient, yielding only one equation for the three unknowns in (104). To solve (104) uniquely, we use the conservation laws (30) and (31) to provide further constraints. Substitution of (67) into (30) and (31) yields

$$\int_0^L (S_j + G_j)\, dx = 0 \tag{105}$$

$$\int_0^L \theta_j\, dx = 0 \tag{106}$$

for all $j \geqslant 1$. Our choice of $L = 2n\pi/k_c$ and $j = 2$ means that

$$v_1^{(2)} + v_2^{(2)} = v_3^{(2)} = 0.$$

Using these constraints, (104) gives

$$v_1^{(2)} = -q_1^{(2)}/(k_+ + k_-).$$

At $\mathcal{O}(\epsilon^3)$ we have

$$\boldsymbol{L}\begin{pmatrix} S_3 \\ G_3 \\ \theta_3 \end{pmatrix} + \boldsymbol{N}_3 + \boldsymbol{E}_3 = \boldsymbol{0}, \tag{107}$$

where

$$\boldsymbol{N}_3 = \begin{pmatrix} F_{S\theta}(S_1\theta_2 + S_2\theta_1) + F_{G\theta}(G_1\theta_2 + G_2\theta_1) \\ -F_{S\theta}(S_1\theta_2 + S_2\theta_1) - F_{G\theta}(G_1\theta_2 + G_2\theta_1) \\ \dfrac{\partial}{\partial x}\left(-\beta G_1 \dfrac{\partial^2\theta_2}{\partial x^2} - \beta G_2 \dfrac{\partial^2\theta_1}{\partial x^2} + H_{G\theta}(G_1\theta_2 + G_2\theta_1)\right. \\ \left. + H_{\theta\theta}\theta_1\theta_2 + H_{G\theta\theta}G_1\theta_1^2/2 + H_{\theta\theta\theta}\theta_1^3/6\right) \end{pmatrix}$$

and

$$\boldsymbol{E}_3 = \begin{pmatrix} \dfrac{\partial S_1}{\partial T} + \dfrac{\partial \theta_1}{\partial T} k_-/k_+ \\ \dfrac{\partial G_1}{\partial T} + \dfrac{\partial \theta_1}{\partial T} - \nu \dfrac{\partial^2 G_1}{\partial x^2} \\ \dfrac{\partial}{\partial x}\left(\dfrac{\partial \theta_1}{\partial T}\right) \end{pmatrix}.$$

Anticipating that secular terms may arise from $\boldsymbol{N}_3 + \boldsymbol{E}_3$, we solve the adjoint problem,

$$\boldsymbol{L}^*\begin{pmatrix} S^* \\ G^* \\ \theta^* \end{pmatrix} = \boldsymbol{0},$$

where L^* is the adjoint of L (64), to prepare for application for the orthogonality condition (70). Solutions are of the form

$$\begin{pmatrix} S^* \\ G^* \\ \theta^* \end{pmatrix} = \beta_1(T)W \exp(ik_c x) + \beta_2(T)\overline{W} \exp(-ik_c x), \tag{108}$$

where $\beta_1(T)$ and $\beta_2(T)$ are arbitrary and

$$W = \begin{pmatrix} 1 \\ w_2 \\ w_3 \end{pmatrix}$$

is the eigenvector given by $\overline{L_{k_c}}^T W = \mathbf{0}$. Thus

$$w_2 = k_c^2/k_+ + 1$$

and

$$-ik_c w_3 = (k_- - (D_c k_c^2 + k_-)(k_c^2/k_+ + 1))/H_G.$$

Equation (108) indicates that terms of the form $\exp(\pm ik_c x)$ give rise to a secular solution ot the $\mathcal{O}(\epsilon^3)$ equation (107). We proceed by isolating these terms. Thus

$$\begin{aligned} N_3 + E_3 = {} & \boldsymbol{R}^{(1)}\alpha|\alpha|^2 \exp(ik_c x) + \overline{\boldsymbol{R}^{(1)}}\bar{\alpha}|\alpha|^2 \exp(-ik_c x) \\ & + \nu \boldsymbol{R}^{(2)}\alpha \exp(ik_c x) + \nu\overline{\boldsymbol{R}^{(2)}}\bar{\alpha} \exp(-ik_c x) \\ & + \boldsymbol{R}^{(3)} \frac{d\alpha}{dT} \exp(ik_c x) + \overline{\boldsymbol{R}^{(3)}} \frac{d\bar{\alpha}}{dT} \exp(-ik_c x) + \text{n.s.t.}, \end{aligned}$$

where

$$\boldsymbol{R}^{(1)} = \begin{bmatrix} F_{S\theta}(u_1 v_3^{(2)} + u_1 v_3^{(1)} + v_1^{(2)} + v_1^{(1)}) \\ \quad + F_{G\theta}(u_2 v_3^{(2)} + u_2 v_3^{(1)} + v_2^{(2)} + v_2^{(1)}) \\ -F_{S\theta}(u_1 v_3^{(2)} + u_1 v_3^{(1)} + v_1^{(2)} + v_1^{(1)}) \\ -F_{G\theta}(u_2 v_3^{(2)} + u_2 v_3^{(1)} + v_2^{(2)} + v_2^{(1)}) \\ ik_c(k_c^2\beta(4u_2 v_3^{(1)} + v_2^{(2)} + v_2^{(1)}) + H_{G\theta}(u_2 v_3^{(2)} + u_2 v_3^{(1)} + v_2^{(2)} + v_2^{(1)}) \\ \quad + H_{\theta\theta}(v_3^{(2)} + v_3^{(1)}) + 3H_{G\theta\theta}u_2/2 + H_{\theta\theta\theta}/2), \end{bmatrix},$$

$$\boldsymbol{R}^{(2)} = \begin{pmatrix} 0 \\ k_c^2 u_2 \\ 0 \end{pmatrix},$$

$$\boldsymbol{R}^{(3)} = \begin{pmatrix} u_1 + k_-/k_+ \\ u_2 + 1 \\ ik_c \end{pmatrix},$$

and n.s.t. indicates terms that do not give rise to a secular solution.

By choosing $\beta_1(T) = 0$ in (108), the orthogonality condition (70) yields

$$\boldsymbol{R}^{(1)} \cdot \overline{\boldsymbol{W}}\alpha|\alpha|^2 + \nu \boldsymbol{R}^{(2)} \cdot \overline{\boldsymbol{W}}\alpha + \boldsymbol{R}^{(3)} \cdot \overline{\boldsymbol{W}} \frac{d\alpha}{dT} = 0, \tag{109}$$

while the choice of $\beta_2(T) = 0$ yields

$$\overline{\boldsymbol{R}^{(1)}} \cdot \boldsymbol{W}\bar{\alpha}|\alpha|^2 + \nu \overline{\boldsymbol{R}^{(2)}} \cdot \boldsymbol{W}\bar{\alpha} + \overline{\boldsymbol{R}^{(3)}} \cdot \boldsymbol{W} \frac{d\bar{\alpha}}{dT} = 0. \tag{110}$$

Thus, solutions satisfying (109) (or its complex conjugate (110)) do not give rise to secular terms.

Multiplying (109) by $\bar{\alpha}$ and adding it to (110) multiplied by α gives

$$\frac{1}{2}\frac{d|\alpha|^2}{dT} = \nu X|\alpha|^2 - Y|\alpha|^4, \tag{111}$$

where

$$X = -\Re\left(\frac{\boldsymbol{R}^{(2)} \cdot \overline{\boldsymbol{W}}}{\boldsymbol{R}^{(3)} \cdot \overline{\boldsymbol{W}}}\right), \tag{112}$$

$$Y = \Re\left(\frac{\boldsymbol{R}^{(1)} \cdot \overline{\boldsymbol{W}}}{\boldsymbol{R}^{(3)} \cdot \overline{\boldsymbol{W}}}\right). \tag{113}$$

This Landau equation predicts the amplitude of $|\alpha|$.

Using (61), we calculate

$$\boldsymbol{R}^{(2)} \cdot \overline{\boldsymbol{W}} = -\frac{\partial C/\partial D(k_c^2)}{H_G k_+}.$$

Equation (40) yields

$$\boldsymbol{R}^{(3)} \cdot \overline{\boldsymbol{W}} = -\frac{B(k_c^2)|_{D=D_c}}{H_G k_+}.$$

Thus Eq. (60) gives

$$X = \frac{\partial \sigma}{\partial D}(k_c^2, D_c),$$

and the linear term in (109) is commensurate with the linear behaviour predicted by (62) and (60).

Appendix B Nonlinear analysis of dispersive wave pattern formation

Substitution of (88) into (84) results in a hierarchy of linear equations for increasing powers of ϵ. Through solving these equations for the first three powers of ϵ we calculate the coefficients, X and Y, of the Landau equation (128) and the components of ϕ (91).

We define the matrix $L_k(z)$ as arising from the action $\boldsymbol{L}$ on terms of the form $\exp(ikz)$. For example,

$$L_k(z_1) = \begin{bmatrix} i\frac{k}{k_c}\sigma_c + k^2 + k_+ & -k_- & i\frac{k}{k_c}\sigma_c\frac{k_-}{k_+} + F_\theta \\ -k_+ & i\frac{k}{k_c}\sigma_c + k_- & i\frac{k}{k_c}\sigma_c - F_\theta \\ 0 & ikH_G & ik\left(i\frac{k}{k_c}\sigma_c + H_\theta\right) \end{bmatrix}. \quad (114)$$

At $\mathcal{O}(\epsilon)$ we have

$$\boldsymbol{L}\begin{pmatrix} S_1 \\ G_1 \\ \theta_1 \end{pmatrix} = \boldsymbol{0}.$$

Therefore solutions are of the form

$$\begin{pmatrix} S_1 \\ G_1 \\ \theta_1 \end{pmatrix} = \alpha_0 a(T)\boldsymbol{U}^{(1)}\exp(ik_c z_1) + \alpha_1 \bar{a}(T)\boldsymbol{U}^{(2)}\exp(-ik_c z_1)$$

$$+ \alpha_2 \bar{a}(T)\boldsymbol{U}^{(3)}\exp(ik_c z_2) + \alpha_3 a(T)\boldsymbol{U}^{(4)}\exp(-ik_c z_2), \quad (115)$$

where $\alpha_0, \ldots, \alpha_3$ are arbitrary constants and

$$L_{k_c}(z_1)\boldsymbol{U}^{(1)} = L_{-k_c}(z_1)\boldsymbol{U}^{(2)} = L_{k_c}(z_2)\boldsymbol{U}^{(3)} = L_{-k_c}(z_2)\boldsymbol{U}^{(4)} = 0.$$

Thus

$$\boldsymbol{U}^{(4)} = \boldsymbol{U}^{(1)} = \boldsymbol{U}$$

and

$$\boldsymbol{U}^{(3)} = \boldsymbol{U}^{(2)} = \bar{\boldsymbol{U}},$$

where

$$\boldsymbol{U} = \begin{pmatrix} u_1 \\ u_2 \\ 1 \end{pmatrix}$$

is the eigenvector given by $L_{k_c}(z_1)\boldsymbol{U} = \boldsymbol{0}$.

To keep the solution real, we choose $\alpha_1 = \bar{\alpha}_0$ and $\alpha_2 = \bar{\alpha}_3$. Application of the zero-gradient boundary conditions for S (28) and G (29) and the conservation law for θ (30) constrains $\alpha_3 = \alpha_0$, making $\gamma = 1/2$ in (78). Therefore, we write the solution (115) as

$$\begin{pmatrix} S_1 \\ G_1 \\ \theta_1 \end{pmatrix} = \alpha\boldsymbol{U}(\exp(ik_c z_1) + \exp(-ik_c z_2)) + \bar{\alpha}\bar{\boldsymbol{U}}(\exp(-ik_c x_1) + \exp(ik_c z_2)), \quad (116)$$

where $\alpha = \alpha_0 a(T)$ and

$$u_1 = (\sigma_c^2 + i\sigma_c(H_G - H_\theta - k_-) - H_G F_\theta - k_- H_\theta)/(k_+ H_G) \tag{117}$$

$$u_2 = -(i\sigma_c + H_\theta)/H_G. \tag{118}$$

At $\mathcal{O}(\epsilon^2)$ we have

$$\boldsymbol{L}\begin{pmatrix} S_2 \\ G_2 \\ \theta_2 \end{pmatrix} + \boldsymbol{N}_2 = \boldsymbol{0},$$

where

$$\boldsymbol{N}_2 = \begin{bmatrix} \dfrac{\sigma_c}{k_c}\left(S_1\left(\dfrac{\partial}{\partial z_1} - \dfrac{\partial}{\partial z_2}\right)\theta_1 + \left(\dfrac{\partial}{\partial z_1} + \dfrac{\partial}{\partial z_2}\right)S_1 \cdot \left(\dfrac{\partial}{\partial z_1} - \dfrac{\partial}{\partial z_2}\right)\int \theta_1\, dx\right) \\ + F_{S\theta} S_1 \theta_1 + F_{G\theta} G_1 \theta_1 \\ \dfrac{\sigma_c}{k_c}\left(G_1\left(\dfrac{\partial}{\partial z_1} - \dfrac{\partial}{\partial z_2}\right)\theta_1 + \left(\dfrac{\partial}{\partial z_1} + \dfrac{\partial}{\partial z_2}\right)G_1 \cdot \left(\dfrac{\partial}{\partial z_1} - \dfrac{\partial}{\partial z_2}\right)\int \theta_1\, dx\right) \\ - F_{S\theta} S_1 \theta_1 - F_{G\theta} G_1 \theta_1 \\ \left(\dfrac{\partial}{\partial z_1} + \dfrac{\partial}{\partial z_2}\right)\left(\dfrac{\sigma_c}{k_c} G_1\left(\dfrac{\partial}{\partial z_1} - \dfrac{\partial}{\varphi z_2}\right)\theta_1 + H_{G\theta} G_1 \theta_1 + H_{\theta\theta}\theta_1^2/2\right) \end{bmatrix}$$

$$\begin{aligned} &= \boldsymbol{Q}^{(1)}\alpha^2 \exp(2ik_c z_1) + \overline{\boldsymbol{Q}^{(1)}}\bar{\alpha}^2 \exp(-2ik_c z_1) \\ &+ \boldsymbol{Q}^{(2)}\alpha^2 \exp(-2ik_c z_2) + \overline{\boldsymbol{Q}^{(2)}}\bar{\alpha}^2 \exp(2ik_c z_2) \\ &+ \boldsymbol{Q}^{(3)}\alpha^2 \exp(ik_c(z_1 - z_2)) + \overline{\boldsymbol{Q}^{(3)}}\bar{\alpha}^2 \exp(-ik_c(z_1 - z_2)) \\ &+ \boldsymbol{Q}^{(4)}|\alpha|^2 \exp(ik_c(z_1 + z_2)) + \overline{\boldsymbol{Q}^{(3)}}|\alpha|^2 \exp(-ik_c(z_1 + z_2)) + \boldsymbol{Q}^{(5)}|\alpha|^2, \end{aligned}$$

for

$$\boldsymbol{Q}^{(i)} = \begin{pmatrix} q_1^{(i)} \\ q_2^{(i)} \\ q_3^{(i)} \end{pmatrix}, \quad 1 \leqslant i \leqslant 5,$$

with components

$$\begin{aligned} q_1^{(1)} &= 2i\sigma_c u_1 + u_1 F_{S\theta} + u_2 F_{G\theta} \\ q_2^{(1)} &= 2i\sigma_c u_2 - u_1 F_{S\theta} - u_2 F_{G\theta} \\ q_3^{(1)} &= -2k_c\sigma_c u_2 + 2ik_c(u_2 H_{G\theta} + H_{\theta\theta}/2) \\ q_1^{(2)} &= q_1^{(1)}, \qquad q_2^{(2)} = q_2^{(1)}, \qquad q_3^{(2)} = -q_3^{(1)} \\ q_1^{(3)} &= 2(u_1 F_{S\theta} + u_2 F_{G\theta}) \\ q_2^{(3)} &= -2(u_1 F_{S\theta} + u_2 F_{G\theta}) \\ q_3^{(3)} &= 0 \end{aligned}$$

$$q_1^{(4)} = 2\Re\{q_1^{(3)} - q_1^{(1)}\}, \qquad q_2^{(4)} = 2\Re\{q_2^{(3)} - q_2^{(1)}\}, \qquad q_3^{(4)} = -2\Im\{q_3^{(3)} - q_3^{(1)}\}$$

$$q_1^{(5)} = \Re\{q_1^{(3)}\}, \qquad q_2^{(5)} = \Re\{q_1^{(3)}\}, \qquad q_3^{(5)} = 0.$$

Thus

$$\begin{pmatrix} S_2 \\ G_2 \\ \theta_2 \end{pmatrix} = \alpha_1 \boldsymbol{U}(\exp(ik_c z_1) + \exp(-ik_c z_2)) + \bar{\alpha}_1 \bar{\boldsymbol{U}}(\exp(-ik_c z_1) + \exp(ik_c z_2))$$

$$+ \boldsymbol{V}^{(1)}\alpha^2 \exp(2ik_c z_1) + \overline{\boldsymbol{V}^{(1)}}\bar{\alpha}^2 \exp(-2ik_c z_1)$$
$$+ \boldsymbol{V}^{(2)}\alpha^2 \exp(-2ik_c z_2) + \overline{\boldsymbol{V}^{(2)}}\bar{\alpha}^2 \exp(2ik_c z_2)$$
$$+ \boldsymbol{V}^{(3)}\alpha^2 \exp(ik_c(z_1 - z_2)) + \overline{\boldsymbol{V}^{(3)}}\bar{\alpha}^2 \exp(-ik_c(z_1 - z_2))$$
$$+ \boldsymbol{V}^{(4)}|\alpha|^2 \exp(ik_c(z_1 + z_2)) + \overline{\boldsymbol{V}^{(4)}}|\alpha|^2 \exp(-ik_c(z_1 + z_2)) + \boldsymbol{V}^{(5)}|\alpha|^2,$$

where

$$L_{2k_c}(z_1)\boldsymbol{V}^{(1)} + \boldsymbol{Q}^{(1)} = \boldsymbol{0} \tag{119}$$

$$L_{-2k_c}(z_2)\boldsymbol{V}^{(2)} + \boldsymbol{Q}^{(2)} = \boldsymbol{0} \tag{120}$$

$$L_{k_c}(z_1 - z_2)\boldsymbol{V}^{(3)} + \boldsymbol{Q}^{(3)} = \boldsymbol{0} \tag{121}$$

$$L_{k_c}(z_1 + z_2)\boldsymbol{V}^{(4)} + \boldsymbol{Q}^{(4)} = \boldsymbol{0} \tag{122}$$

$$L_0 \boldsymbol{V}^{(5)} + \boldsymbol{Q}^{(5)} = \boldsymbol{0}. \tag{123}$$

These equations, of the form $L\boldsymbol{V} + \boldsymbol{Q} = \boldsymbol{0}$, have the solution $\boldsymbol{V} = -L^{-1}\boldsymbol{Q}$, provided the L is non-singular. However, as calculating L^{-1} is algebraically cumbersome, we take advantage of the zero element in L to write a general solution of the form

$$\boldsymbol{V} = \boldsymbol{V}(L, \boldsymbol{Q}) = \begin{pmatrix} v_1 \\ v_2 \\ v_3 \end{pmatrix},$$

where

$$v_3 = (l_{11}(l_{22}q_3/l_{32} - q_2)/l_{21} - l_{12}q_3/l_{32} + q_1)/(l_{11}(l_{23} - l_{22}l_{33}/l_{32})/l_{21} + l_{12}l_{13}/l_{32} - l_{13}),$$
$$v_2 = -(q_3 + l_{33}v_3)/l_{32},$$
$$v_1 = (l_{22}q_3/l_{32} - q_2 + (l_{22}l_{33}/l_{32} - l_{32})v_3)/l_{21},$$

for

$$\boldsymbol{Q} = \begin{pmatrix} q_1 \\ q_2 \\ q_3 \end{pmatrix}$$

and

$$L = (l_{ij}) \quad 1 \leqslant i, j \leqslant 3.$$

Thus our solutions to (119), (120) and (122) are given by

$$\boldsymbol{V}^{(1)} = \boldsymbol{V}(L_{2k_c}(z_1), \boldsymbol{Q}^{(1)}),$$
$$\boldsymbol{V}^{(2)} = \boldsymbol{V}(L_{-2k_c}(z_2), \boldsymbol{Q}^{(2)}),$$
$$\boldsymbol{V}^{(4)} = \boldsymbol{V}(L_{k_c}(z_1 + z_2), \boldsymbol{Q}^{(4)}).$$

As neither $\alpha^2 \exp(z_1 - z_2)$ nor $|\alpha|^2$ have a space component, we use the conservation laws (105) and (106) to add constraints so that the rank deficient systems (121) and (123) yield unique solutions. The application of (105) and (106) for $j = 2$ and $L = 2n\pi/k_c$ gives

$$(v_1^{(3)} + v_2^{(3)})\alpha^2 \exp(2i\sigma_c t) + (\bar{v}_1^{(3)} + \bar{v}_2^{(3)})\bar{\alpha}^2 \exp(-2i\sigma_c t) + (v_1^{(5)} + v_2^{(5)})|\alpha|^2 = 0$$

and

$$v_3^{(3)}\alpha^2 \exp(2i\sigma_c t) + \bar{v}_3^{(3)}\bar{\alpha}^2 \exp(-2i\sigma_c t) + v_3^{(5)}|\alpha| = 0.$$

As these must hold for arbitrary t, the solution is

$$v_1^{(3)} + v_2^{(3)} = v_3^{(3)} = 0, \qquad v_1^{(5)} + v_2^{(5)} = v_3^{(5)} = 0,$$

yielding

$$v_1^{(3)} = -q_1^{(3)}/(2i\sigma_c + 2k_+), \qquad v_1^{(5)} = -q_1^{(5)}/(k_+ + k_-).$$

At $\mathcal{O}(\epsilon^3)$ we have

$$\boldsymbol{L}\begin{pmatrix} S_3 \\ G_3 \\ \theta_3 \end{pmatrix} + \boldsymbol{N}_3 + \boldsymbol{E}_3 = \boldsymbol{0}, \tag{124}$$

where

$$\boldsymbol{N}_3 = \begin{Bmatrix} \dfrac{\sigma_c}{k_c}\left(S_1\left(\dfrac{\partial}{\partial z_1} - \dfrac{\partial}{\partial z_2}\right)\theta_2 + S_2\left(\dfrac{\partial}{\partial z_1} - \dfrac{\partial}{\partial z_2}\right)\theta_1 \right. \\ \quad + \left(\dfrac{\partial}{\partial z_1} + \dfrac{\partial}{\partial z_2}\right)S_1 \cdot \left(\dfrac{\partial}{\partial z_1} - \dfrac{\partial}{\partial z_2}\right)\int \theta_2\, dx \\ \quad \left. + \left(\dfrac{\partial}{\partial z_1} + \dfrac{\partial}{\partial z_2}\right)S_2 \cdot \left(\dfrac{\partial}{\partial z_1} - \dfrac{\partial}{\partial z_2}\right)\int \theta_1\, dx\right) \\ \quad + F_{S\theta}(S_1\theta_2 + S_2\theta_1) + F_{G\theta}(G_1\theta_2 + G_2\theta_1) \\ \dfrac{\sigma_c}{k_c}\left(G_1\left(\dfrac{\partial}{\partial z_1} - \dfrac{\partial}{\partial z_2}\right)\theta_2 + G_2\left(\dfrac{\partial}{\partial z_1} - \dfrac{\partial}{\partial z_2}\right)\theta_1 \right. \\ \quad + \left(\dfrac{\partial}{\partial z_1} + \dfrac{\partial}{\partial z_2}\right)G_1 \cdot \left(\dfrac{\partial}{\partial z_1} - \dfrac{\partial}{\partial z_2}\right)\int \theta_2\, dx \\ \quad \left. + \left(\dfrac{\partial}{\partial z_1} + \dfrac{\partial}{\partial z_2}\right)G_2 \cdot \left(\dfrac{\partial}{\partial z_1} - \dfrac{\partial}{\partial z_2}\right)\int \theta_1\, dx\right) \\ \quad - F_{S\theta}(S_1\theta_2 + S_2\theta_1) - F_{G\theta}(G_1\theta_2 + G_2\theta_1) \\ \left(\dfrac{\partial}{\partial z_1} + \dfrac{\partial}{\partial z_2}\right)\left(\dfrac{\sigma_c}{k_c}\left(G_1\left(\dfrac{\partial}{\partial z_1} - \dfrac{\partial}{\partial z_2}\right)\theta_2 + G_2\left(\dfrac{\partial}{\partial z_1} - \dfrac{\partial}{\partial z_2}\right)\theta_1\right)\right. \\ \left. + H_{G\theta}(G_1\theta_2 + G_2\theta_1) + H_{\theta\theta}\theta_1\theta_2 + H_{G\theta\theta}G_1\theta_1^2/2 + H_{\theta\theta\theta}\theta_1^3/6\right) \end{Bmatrix}$$

and

$$\boldsymbol{E}_3 = \begin{pmatrix} \dfrac{\partial S_1}{\partial T} + \dfrac{\partial \theta_1}{\partial T} k_-/k_+ \\ \dfrac{\partial G_1}{\partial T} + \dfrac{\partial \theta_1}{\partial T} \\ \left(\dfrac{\partial}{\partial z_1} + \dfrac{\partial}{\partial z_2}\right)\left(\dfrac{\partial \theta_1}{\partial T} + \nu(G_1 + \theta_1)\right) \end{pmatrix}.$$

Anticipating that secular terms may arise from $\boldsymbol{N}_3 + \boldsymbol{E}_3$, We solve the adjoint problem,

$$\boldsymbol{L}^* \begin{pmatrix} S^* \\ G^* \\ \theta^* \end{pmatrix} = \boldsymbol{0},$$

where $\boldsymbol{L}^*$ is the adjoint of $\boldsymbol{L}$ (85) to prepare for application of the orthogonality condition (70). Solutions are of the form

$$\begin{pmatrix} S^* \\ G^* \\ \theta^* \end{pmatrix} = \beta_1(T)\boldsymbol{W}^{(1)} \exp(ik_c z_1) + \beta_2(T)\overline{\boldsymbol{W}^{(1)}} \exp(-ik_c z_1)$$
$$+ \beta_3(T)\overline{\boldsymbol{W}^{(2)}} \exp(ik_c z_2) + \beta_4(T)\boldsymbol{W}^{(2)} \exp(-ik_c z_2), \qquad (125)$$

where $\beta_1(T)$, $\beta_2(T)$, $\beta_3(T)$ and $\beta_4(T)$ are arbitrary and

$$\overline{\boldsymbol{L}_{k_c}}^T(z_1)\boldsymbol{W}^{(1)} = \overline{\boldsymbol{L}_{-k_c}}^T(z_2)\boldsymbol{W}^{(2)} = \boldsymbol{0}.$$

Thus

$$\boldsymbol{W}^{(1)} = \begin{pmatrix} 1 \\ w_2 \\ w_3 \end{pmatrix} \quad \text{and} \quad \boldsymbol{W}^{(2)} = \begin{pmatrix} 1 \\ w_2 \\ -w_3 \end{pmatrix},$$

where

$$w_2 = (-i\sigma_c + k_c^2 + k_+)/k_+$$

and

$$-ik_c w_3 = (\sigma_c^2 + i\sigma_c(k_c^2 + k_- + k_+) - k_- k_c^2)/(H_G k_+).$$

Equation (125) indicates that terms of the form $\exp(\pm ik_c x)$ give rise to a secular solution to the $\mathcal{O}(\varepsilon^3)$ equation (124). We proceed by isolating these terms. Thus

$$\begin{aligned} \boldsymbol{N}_3 + \boldsymbol{E}_3 = {} & \boldsymbol{R}^{(1)}\alpha|\alpha|^2 \exp(ik_c z_1) + \overline{\boldsymbol{R}^{(1)}}\bar{\alpha}|\alpha|^2 \exp(-ik_c z_1) \\ & + \boldsymbol{R}^{(2)}\alpha|\alpha|^2 \exp(-ik_c z_2) + \overline{\boldsymbol{R}^{(2)}}\bar{\alpha}|\alpha|^2 \exp(ik_c z_2) \\ & + \nu\boldsymbol{R}^{(3)}\alpha \exp(ik_c z_1) + \nu\overline{\boldsymbol{R}^{(3)}}\bar{\alpha} \exp(-ik_c z_1) \\ & + \nu\boldsymbol{R}^{(4)}\alpha \exp(-ik_c z_2) + \nu\overline{\boldsymbol{R}^{(4)}}\bar{\alpha} \exp(ik_c z_2) \\ & + \boldsymbol{R}^{(5)}\frac{\partial \alpha}{\partial T} \exp(ik_c z_1) + \overline{\boldsymbol{R}^{(5)}}\frac{\partial \bar{\alpha}}{\partial T} \exp(-ik_c z_1) \\ & + \boldsymbol{R}^{(6)}\frac{\partial \alpha}{\partial T} \exp(-ik_c z_2) + \overline{\boldsymbol{R}^{(6)}}\frac{\partial \bar{\alpha}}{\partial T} \exp(ik_c z_2) + \text{n.s.t.} \end{aligned}$$

We write the vector components of $\boldsymbol{R}^{(i)}$ as

$$\boldsymbol{R}^{(i)} = \begin{pmatrix} r_1^{(i)} \\ r_2^{(i)} \\ r_3^{(i)} \end{pmatrix}, \quad 1 \leqslant i \leqslant 6.$$

Thus $\boldsymbol{R}^{(1)}$ is given by

$$\begin{aligned}
r_1^{(1)} &= i\sigma_c(\bar{u}_1(v_3^{(1)} + 2v_3^{(3)}) + v_1^{(5)} - v_1^{(4)} + v_1^{(1)} - v_1^{(3)}) \\
&\quad + F_{S\theta}(u_1(v_3^{(5)} + v_3^{(4)}) + \bar{u}_1(v_3^{(1)} + v_3^{(3)}) + v_1^{(5)} + v_1^{(4)} + v_1^{(3)} + v_1^{(1)}) \\
&\quad + F_{G\theta}(u_2(v_3^{(5)} + v_3^{(4)}) + \bar{u}_2(v_3^{(1)} + v_3^{(3)}) + v_2^{(5)} + v_2^{(4)} + v_2^{(3)} + v_2^{(1)}) \\
r_2^{(1)} &= i\sigma_c(\bar{u}_2(v_3^{(1)} + 2v_3^{(3)}) + v_2^{(5)} - v_2^{(4)} + v_2^{(1)} - v_2^{(3)}) \\
&\quad - F_{S\theta}(u_1(v_3^{(5)} + v_3^{(4)}) + \bar{u}_1(v_3^{(1)} + v_3^{(3)}) + v_1^{(5)} + v_1^{(4)} + v_1^{(3)} + v_1^{(1)}) \\
&\quad - F_{G\theta}(u_2(v_3^{(5)} + v_3^{(4)}) + \bar{u}_2(v_3^{(1)} + v_3^{(3)}) + v_2^{(5)} + v_2^{(4)} + v_2^{(3)} + v_2^{(1)}) \\
r_3^{(1)} &= -k_c\sigma_c(2\bar{u}_2(v_3^{(1)} + v_3^{(3)}) + v_2^{(5)} + v_2^{(4)} - v_2^{(3)} - v_2^{(1)}) \\
&\quad + ik_c(H_{G\theta}(u_2(v_3^{(5)} + v_3^{(4)}) + \bar{u}_2(v_3^{(1)} + v_3^{(3)}) + v_2^{(5)} + v_2^{(4)} + v_2^{(3)} + v_2^{(1)}) \\
&\quad + H_{\theta\theta}(v_3^{(5)} + v_3^{(4)} + v_3^{(3)} + v_3^{(1)}) + 3H_{G\theta\theta}(2u_2 + \bar{u}_2)/2 + 3H_{\theta\theta\theta}/2).
\end{aligned}$$

We calculate the components of $\boldsymbol{R}^{(2)}$ as

$$r_1^{(2)} = r_1^{(1)}, \qquad r_2^{(2)} = r_2^{(1)}, \qquad r_3^{(2)} = -r_3^{(1)},$$

where we have used the fact that $\boldsymbol{V}^{(4)} - \overline{\boldsymbol{V}^{(4)}} = \boldsymbol{V}^{(1)} - \boldsymbol{V}^{(2)} = 0$. The components $\boldsymbol{R}^{(3)}$ through $\boldsymbol{R}^{(6)}$ are calculated as

$$\begin{aligned}
&r_1^{(3)} = 0, \qquad r_2^{(3)} = 0, \qquad r_3^{(3)} = ik_c(1 + u_2), \\
&r_1^{(4)} = r_1^{(3)}, \qquad r_2^{(4)} = r_2^{(3)}, \qquad r_3^{(4)} = -r_3^{(3)}, \\
&r_1^{(5)} = u_1 + k_-/k_+, \qquad r_2^{(5)} = u_2 + 1, \qquad r_3^{(5)} = ik_c, \\
&r_1^{(6)} = r_1^{(5)}, \qquad r_2^{(6)} = r_2^{(5)}, \qquad r_3^{(6)} = -r_3^{(5)}.
\end{aligned}$$

By choosing $\beta_1(T) = \beta_3(T) = \beta_4(T) = 0$ in (125), the orthogonality condition (70) yields

$$\boldsymbol{R}^{(1)} \cdot \overline{\boldsymbol{W}^{(1)}}\alpha|\alpha|^2 + \nu\boldsymbol{R}^{(3)} \cdot \overline{\boldsymbol{W}^{(1)}}\alpha + \boldsymbol{R}^{(5)} \cdot \overline{\boldsymbol{W}^{(1)}}\frac{d\alpha}{dT} = 0, \tag{126}$$

while the choice of $\beta_2(T) = \beta_3(T) = \beta_4(T) = 0$ yields

$$\overline{\boldsymbol{R}^{(1)}} \cdot \boldsymbol{W}^{(1)}\bar{\alpha}|\alpha|^2 + \nu\overline{\boldsymbol{R}^{(3)}} \cdot \boldsymbol{W}^{(1)}\bar{\alpha} + \overline{\boldsymbol{R}^{(5)}} \cdot \boldsymbol{W}^{(1)}\frac{d\bar{\alpha}}{dT} = 0. \tag{127}$$

The choice of $\beta_3(T)$ or $\beta_4(T)$ as the non-zero coefficients yields two further equations that are identical to (126) and (127), once the vector products are multiplied out. Thus, solutions satisfying (126) (or its complex conjugate (127)) do not give rise to secular terms.

Using (56), (52), (54) and (82) we calculate

$$\boldsymbol{R}^{(3)} \cdot \overline{\boldsymbol{W}^{(1)}} = -\frac{\dfrac{\partial C}{\partial \pi}(k_c^2) + i\sigma_c\dfrac{\partial B}{\partial \pi}(k_c^2)}{H_G k_+}.$$

Equations (56), (52), (53), and (54) yield

$$\boldsymbol{R}^{(5)} \cdot \overline{\boldsymbol{W}^{(1)}} = \frac{2(B(k_c^2) - i\sqrt{A(k_c^2)C(k_c^2)})|_{\pi=\pi_c}}{H_G k_+}.$$

Thus the linear term in (126) is commensurate with the linear behaviour predicted by (83) and (81).

Multiplying (126) by $\bar{\alpha}$ and adding it to (127) multiplied by α finally gives

$$\frac{1}{2}\frac{d|\alpha|^2}{dT} = \nu X|\alpha|^2 - Y|\alpha|^4 \tag{128}$$

where

$$X = -\Re\left(\frac{\boldsymbol{R}^{(3)} \cdot \overline{\boldsymbol{W}^{(1)}}}{\boldsymbol{R}^{(5)} \cdot \overline{\boldsymbol{W}^{(1)}}}\right), \tag{129}$$

$$Y = \Re\left(\frac{\boldsymbol{R}^{(1)} \cdot \overline{\boldsymbol{W}^{(1)}}}{\boldsymbol{R}^{(5)} \cdot \overline{\boldsymbol{W}\mathrm{a}^{(1)}}}\right). \tag{130}$$

This Landau equation predicts the amplitude of $|\alpha|$ in the $\mathcal{O}(\epsilon)$ equation (116).

Acknowledgments. MAL would like to acknowledge support provided by a PDF 1 fellowship from NSERC of Canada. JDM was supported in part by Grant DMS-9003339 from the US National Science Foundation.

References

Abercrombie, M., Heaysman, J. E. M., Pegrum, S. M.: The locomotion of fibroblasts in culture. II. 'Ruffling'. Exp. Cell Res. **60**, 437–444 (1970)

Alberts, B., Bray, D., Lewis, J., Raff, M., Roberts, K., Watson, J. D.: Molecular Biology of the Cell. London: Garland 1983

Argiro, V., Bunge, M. B., Johnson, M. L.: A quantitative study of growth cone filopodial extension. J. Neurosci. Res. **13**, 149–162 (1985)

Bray, D., White, J. G.: Cortical flow in animal cells. Science **239**, 883–888 (1988)

Cohan, C. S., Connor, J. A., Kater, S. B.: Electrically and chemically mediated increases in intracellular calcium in neuronal growth cones. J. Neurosci. **7** (11), 3588–3599 (1987)

Condeelis, J.: Rheological properties of cytoplasm: significance for the organization of spatial information and movement. In: McIntosh, J. (ed.) Modern Cell Biology, vol. 2: Spatial Organization of Eucaryotic Cells, pp. 225–240. New York: Alan R. Liss 1983

Connor, J. A.: Digital imaging of free calcium changes and of spatial gradients in growing processes in single, mammalian central nervous system cells. Proc. Natl. Acad. Sci. USA **83**, 6179–6183 (1986)

Forscher, P.: Calcium and polyphosphinositide control of cytoskeletal dynamics. Trends Neurosci. **12** (11), 468–474 (1989)

Forscher, P., Smith, S. J.: Actions of cytochalasins on the organization of actin filaments and microtubules in a neuronal growth cone. J. Cell Biol. **107**, 1505–1516 (1988)

Gordon-Weeks, P. R.: GAP-43 – What does it do in the growth cone? Trends Neurosci. **12** (10), 363–365 (1989)

Harris, A. K.: Cell surface movements related to cell locomotion. (Ciba Found. Symp., New Ser. 14, pp. 3–26) Amsterdam: Associated Scientific Publishers 1973

Hudspeth, A. J.: The hair cells of the inner ear. Sci. Am. **248**, 42–52 (1983)

Kater, S. B., Mattson, M. P., Cohan, C., Connor, J.: Calcium regulation of the neuronal growth cone. Trends Neurosci. **11** (7), 315–321 (1988)

Landau, L. D., Lifshitz, E. M.: Theory of Elasticity, 2nd ed. London: Pergamon 1970

Lewis, M. A.: Analysis of Dynamic and Stationary Biological Pattern Formation. D.Phil. Thesis, University of Oxford (1990)

Lewis, M. A., Murray, J. D.: Analysis of stable two-dimensional patterns in contractile cytogel. J. Nonlin. Sci. **1**, 289–311 (1991)

Lur'e, A. I.: Three-Dimensional Problems of the Theory of Elasticity, chap. 1. New York: John Wiley 1964

Matkowski, B. J.: Nonlinear dynamic stability. SIAM J. Appl. Math. **18**, 872–883 (1970)

Murray, J. D.: Parameter space for Turing instability in reaction diffusion mechanisms: A comparison of models. J. Theor. Biol. **99**, 161–199 (1982)

Murray, J. D.: Mathematical Biology. Berlin Heidelberg New York: Springer 1989

Odell, G. M.: A mathematically modelled cytogel cortex exhibits periodic Ca^{++}-modulated contraction cycles seen in *Physarum* shuttle streaming. J. Embryol. Exp. Morphol. **83**, 261–287 (1984)

Oster, G. F.: On the crawling of cells. J. Embryol. Exp. Morphol. **83**, 329–364 (1984)

Oster, G. F., Murray, J. D., Harris, A. K.: Mechanical aspects of mesenchymal morphogenesis. J. Embryol. Exp. Morphol. **78**, 83–125 (1983)

Oster, G. F., Murray, J. D., Odell, G. M.: The formation of microvilli. In: Molecular Determinants of Animal Form, pp. 365–384. New York: Alan R. Liss 1985

Oster, G. F., Odell, G. M.: Mechanics of cytogels I: Oscillations in *Physarum*. Cell Motil. **4**, 469–503 (1984a)

Oster, G. F., Odell, G. M.: The mechanochemistry of cytogels. Physica **12D**, 333–350 (1984b)

Purcell, E.: Life at Low Reynolds Number. Am. J. Phys. **45**, 1–11 (1977)

Silver, R. A., Lamb, A. G., Bolsover, S. R.: Calcium hotspots caused by L-channel clustering promote morphological changes in neuronal growth cones. Nature **343**, 751–754 (1990)

Stossel, T. P.: The spatial organization of cortical cytoplasm in macrophages. In: McIntosh, J. (ed.) Modern Cell Biology, vol. 2: Spatial Organization of Eucaryotic Cells, pp. 203–223. New York: Alan R. Liss 1983

Tanaka, T.: Gels. Sci. Am. **244** (1), 124–138 (1981)

Taylor D., Hellewell, S., Virgin, H., Heiple, J.: The solation-contraction coupling hypothesis of cell movements. In: Hatano, S. (ed.) Cell Motility, pp. 363–377. Baltimore: University Park Press 1979

Tilney, L. G.: The role of actin in nonmuscle cell motility. In Inoué, S., Stephens, R. E. (eds.) Molecules and Cell Movement, pp. 339–388. New York: Raven 1975

Tilney, L. G., De Rosier, D. J.: Actin filaments, stereocilia and hair cells of the bird cochlea IV. How the actin filaments become organized in developing stereocilia and in the cuticular plate. Dev. Biol. **116**, 119–129 (1986)

Tilney, L. G., Inoué, S.: Acrosomal reaction of *Thyrone* sperm. II. The kinetics and possible mechanism of acrosomal process elongation. J. Cell Biol. **93**, 820–827 (1982)

Tosney, K. W., Wessells, N. K.: Neuronal motility: The ultrastructure of veils and microspikes correlates with their motile activities. J. Cell Sci. **61**, 389–411 (1983)

Weeds, A.: Actin-binding proteins – regulators of cell architecture and motility. Nature **296**, 811–816 (1982)

Zuber, M. X., Goodman, D. W., Karns, L. R., Fishman, M. C.: The neuronal growth-associated protein GAP-43 induces filopodia in non-neuronal cells. Science **244**, 1193–1195 (1989)